

Geochemical and Sr–Nd isotopic constraints on the petrogenesis and geodynamic significance of the Jebilet magmatism (Variscan Belt, Morocco)

ABDERRAHIM ESSAIFI*†, SCOTT SAMSON‡ & KATHRYN GOODENOUGH§

*Geology Department, Cadi Ayyad University, B.P. 2390, Marrakech 40000, Morocco

‡Department of Earth Sciences, Syracuse University, Syracuse, NY 13244, USA

§British Geological Survey, Murchison House, West Mains Road, Edinburgh EH9 3LA, UK

(Received 20 December 2012; accepted 10 July 2013; first published online 20 September 2013)

Abstract – In the Variscan fold belt of Morocco, the Jebilet massif is characterized by Palaeozoic metasedimentary rocks intruded by syntectonic magmatism that includes an ultramafic–granitoid bimodal association and peraluminous granodiorites emplaced *c.* 330 Ma, intruded by younger leucogranites *c.* 300 Ma. The mafic–ultramafic rocks belong to a tholeiitic series, and display chemical and isotopic signatures consistent with mixing between mantle-derived and crust-derived magmas or assimilation and fractional crystallization. The granites within the bimodal association are mainly metaluminous to weakly peraluminous microgranites that show characteristics of A₂-type granites. The peraluminous, calc-alkaline series consists mainly of cordierite-bearing granodiorites enclosing magmatic microgranular enclaves and pelitic xenoliths. Detailed element and isotope data suggest that the alkaline and the peraluminous granitoids were formed in the shallow crust (<30 km) by partial melting of tonalitic sources at high temperatures (up to 900 °C) and by partial melting of metasedimentary protoliths at relatively low temperatures (*c.* 750 °C), respectively. Mixing between the coeval mantle-derived and crust-derived magmas contributed to the large variation of initial ϵ_{Nd} values and initial Sr isotopic ratios observed in the granitoids. Further contamination occurred by wall-rock assimilation during ascent of the granodioritic plutons to the upper crust. The ultramafic–granitoid association has been intruded by leucogranites that have high initial Sr isotopic ratios and low initial ϵ_{Nd} values, indicating a purely crustal origin. The heating events that caused emplacement of the Jebilet magmatism are related to cessation of continental subduction and convective erosion/thinning of the lithospheric mantle during plate convergence.

Keywords: bimodal magmatism, peraluminous granite, Sr–Nd isotopes, Variscan orogeny, Morocco.

1. Introduction

Magmatic rocks found in orogenic belts provide a record of the thermal and chemical evolution of the deep lithospheric root of the developing orogen. During the evolution of continental collision zones, the convergence is typically first accommodated by thrusts leading to lithospheric thickening and then by crustal-scale shear zones leading to synconvergent exhumation and lateral extrusion. Magmas of variable sources and types may be generated during the synconvergence post-thickening period. This type of magmatism, described as post-collisional, comprises a large variety of magmatic rocks including calc-alkaline or peraluminous granitoids and alkaline-type series (Whalen, Currie & Chappell, 1987; Lagarde, Capdevila & Fourcade, 1992; Bonin, 1996; Whalen *et al.* 2006); it is therefore potentially informative of a range of deep crustal processes.

In the Moroccan Variscan belt, the SW extremity of the Variscan orogen of Europe and North Africa, Variscan convergence was mainly accommodated by conjugate transcurrent shear zones that are locally

associated with westward thrusting (Piqué, Jeannette & Michard, 1980; Lagarde & Michard, 1986). Despite this very limited crustal thickening, numerous syntectonic calc-alkaline and peraluminous granitic plutons intruded the Cambrian–Carboniferous sedimentary formations of the Moroccan Meseta (Diot & Bouchez, 1989; Lagarde, Aït Omar & Roddaz, 1990; Gasquet, Stussi & Nachit, 1996). Some of these plutons are associated with coeval mafic rocks (Fig. 1), for example the Tichka massif (Vogel *et al.* 1976; Gasquet *et al.* 1992) and Tanncherfi complex (Ajaji *et al.* 1998), allowing evaluation of crustal- versus mantle-derived source contributions in the genesis of the granitic magmas. The geodynamic context and the thermotectonic event that allowed crust and mantle melting in the Moroccan Meseta remain a subject of discussion. Magmatism was related to subduction and wet melting of the metasomatized mantle lithosphere of the overriding plate (Roddaz *et al.* 2002; El Hadi *et al.* 2006; Michard *et al.* 2010) and/or to partial fusion of the lower crust during a post-collisional intracontinental deformation (Lagarde, 1989; Gasquet, Stussi & Nachit, 1996; Hoepffner *et al.* 2005). In their general plate-tectonic evolution of the SE Variscan belt (von Raumer &

†Author for correspondence: essaifi@uca.ma

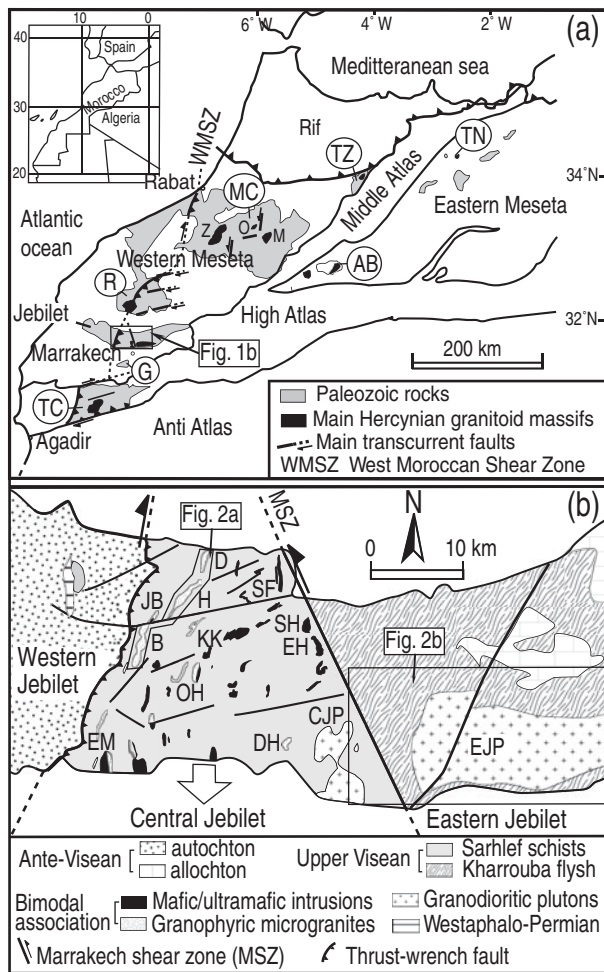


Figure 1. (a) Moroccan Variscan granitoids (black) and their Paleozoic cover (grey) (TN – Tanncherfi; AB – Aouli-Bou Mia; TZ – Tazekka; TC – Tichka; MC – Maroc Central with Zaer (Z), Oulmes (O) and Ment (M) plutons; R – Rehamna; G – Guemassa). (b) Geological sketch map of the Jebilet massif (modified from Huvelin, 1977). Slip on the regional fractures is accompanied by extrusion to the south of the central Jebilet block (large white arrow). BHD – Koudiat Bouzlaf, Hamra and Diab intrusions; DH – Draa El Harach; KK – Koudiat Kettara; OH – Oled Har; SF – Safsafat; SH – Sarhlef; EH – El Harcha; EM – El Mna; JB – Jbel Bouzlaf; CJP – Central Jebilet Pluton; EJP – Eastern Jebilet Pluton.

Stampfli, 2008; von Raumer, Bussy & Stampfli, 2009), the Moroccan Meseta and the Anti-Atlas represent the northern and southern margins of the Palaeotethys, respectively. This ocean was consumed during the Carboniferous by combining N-dipping subduction, dextral strike-slip and collision between the continents of Gondwana and Laurussia.

In the Jebilet massif, the syntectonic magmatic rocks can be divided into two main groups: a bimodal magmatic association including numerous intrusions of tholeiitic mafic–ultramafic rocks and alkaline granophyric microgranites; and calc-alkaline peraluminous granodioritic plutons cut across by leucogranitic dykes. It has been suggested that the bimodal association is mantle-derived, whereas the peraluminous granitoids largely have a source in the upper crust (Aarab &

Beauchamp, 1987; Mrini *et al.* 1992). The presence of these two magmatic groups most likely reflects a systematic interaction between the continental crust and upper mantle in this region during the Variscan orogeny.

In this paper, petrographical, geochemical and isotopic (Rb–Sr, Sm–Nd) data for the different Carboniferous magmatic suites are integrated in order to estimate the composition of the source rocks, to constrain the petrogenesis of the varied magmatic rocks and to evaluate tectonic models for the evolution of the Moroccan Meseta during Late Palaeozoic time.

2. Geological setting and geology of the Jebilet magmatism

2.a. Geological setting

The Jebilet massif, located 7 km north of Marrakech, is one of the largest Palaeozoic massifs of the Variscan fold belt of Morocco. Together with the Rehamna and the central Palaeozoic massifs to the north and the high Atlas Palaeozoic block to the south, it constitutes the western Meseta (separated from the eastern Meseta by the folded Mesozoic–Cenozoic cover of the middle Atlas) (Fig. 1a). The Mesetas display a nearly complete Palaeozoic sedimentary sequence, folded and metamorphosed at greenschist–amphibolite facies, and intruded by widespread syn- to late-orogenic Carboniferous granitoids.

The granitoids of the Mesetas can be grouped into three main groups (Vogel *et al.* 1976; Gasquet, Stussi & Nachit, 1996; El Hadi *et al.* 2006): (1) calc-alkaline biotite±cordierite granodiorites, locally with associated mafic magmas; (2) two-mica leucogranites; and (3) subalkaline–alkaline granites. The calc-alkaline granodioritic plutons are dominant (e.g. Jebilet, Aouli Bou-Mia, Tanncherfi; Fig. 1a). They display I-type or mixed S- and I-type characteristics ($0.703 < Sr_i < 0.711$; $-6.7 < \epsilon_{Nd} < +7.4$) and are locally associated with mantle-derived basic magmas (e.g. Tichka pluton, Fig. 1a). Among these calc-alkaline granitoids, subduction-related plutonic rocks have been recognized in the Tanncherfi plutonic complex where coeval potassic (shoshonitic) and sodic (granodioritic) calc-alkaline series, with large-ion lithophile element (LILE) and light rare Earth element (LREE) enrichment and Nb, Ta, Ti depletion, were emplaced (Ajaji *et al.* 1998). The leucogranites are typical S-type granites ($0.707 < Sr_i < 0.718$; $-10.7 < \epsilon_{Nd} < -1.5$) derived from metasedimentary source rocks (Mahmood & Bennani, 1984; Mrini *et al.* 1992). They are intrusive into the granodiorites (e.g. Zaer pluton, Fig. 1a) or into Lower Palaeozoic metasediments (e.g. Oulmes pluton, Fig. 1a). The subalkaline–alkaline granites ($0.704 < Sr_i < 0.707$; $-4.9 < \epsilon_{Nd} < 0.6$) result from mixing between crust- and mantle-derived magmas (Gasquet, Stussi & Nachit, 1996). They are associated with mafic rocks and coeval with the calc-alkaline granites (e.g. Tichka

massif) or intrusive into Lower Palaeozoic metasediments (e.g. Rehamna, Fig. 1a).

In addition to two cordierite-bearing granodioritic plutons intruded by leucogranites, Carboniferous magmatism in the Jebilet massif includes a compositionally bimodal association of alkaline microgranites and mafic–ultramafic intrusions (Bordonaro, Gaillet & Michard, 1979; Gasquet, Stussi & Nachit, 1996). Its spatial distribution is limited to the west by a NNE–SSW dextral thrust-wrench shear zone (Mayol & Muller, 1985; Le Corre & Boulton, 1987) separating the central Jebilet unit, a schistose and metamorphosed block of marine Visean shales (Sarhlef schists), from the western Jebilet, a weakly deformed to undeformed block of Cambro-Ordovician limestones, shales and sandstones (Fig. 1b) (Huvelin, 1977). To the east, the granodioritic plutons are spatially associated with a NNW–SSE sinistral wrench shear zone (the Marrakech Shear Zone, Lagarde & Choukroune, 1982; Essaifi, Lagarde & Capdevila, 2001) corresponding to the boundary with the eastern Jebilet, a weakly metamorphosed to unmetamorphosed block of upper Visean syntectonic ‘flysch’ with olistostromes and inliers of Ordovician–Devonian sedimentary rocks (Huvelin, 1977; Beauchamp, Izart & Piqué, 1991). These two shear zones are located in the southern prolongation of the western Meseta shear zone (WMSZ, Fig. 1a), which is the western boundary of the Carboniferous basins of the Moroccan Meseta (Piqué, Jeannette & Michard, 1980). Westphalian–Permian continental conglomerates (Huvelin, 1977) rest unconformably upon the Hercynian folded sequence.

Both the cordierite-bearing granodioritic plutons and the bimodal plutonic suite intrude weakly metamorphosed (lower greenschist facies) marine metapelites dated to upper–middle Visean (Huvelin, 1977; Playford *et al.* 2008). Structural studies of the Jebilet plutons and the surrounding rocks have provided evidence of syntectonic emplacement at high crustal levels for both the bimodal association and the granodioritic plutons (Le Corre & Saquaque, 1987; Lagarde, Aït Omar & Roddaz, 1990; Essaifi, Lagarde & Capdevila, 2001). Regional metamorphism was contemporaneous with ductile deformation developed during Late Carboniferous crustal shortening, associated with the main Variscan tectonic event in Morocco (Hoepffner *et al.* 2005; Michard *et al.* 2010). The bimodal intrusions and the granodioritic plutons have induced in the surrounding metapelites a low-pressure contact metamorphism that reaches the hornblende- and the pyroxene-hornfels facies, respectively (Fig. 2a, b). Near the boundaries with the host rocks, numerous centimetre- to kilometre-scale enclaves of the contact hornfels exist in the eastern Jebilet granodioritic pluton. The contact metamorphism paragenesis suggests that the plutons were emplaced at less than 2.2 kbar corresponding to a maximum depth of 8 km (Boulton, 1992). Leucogranitic dykes and stocks cut across the granodioritic plutons and their host rocks. Triassic microdioritic dykes post-date the Variscan deformation and cut both the bimodal

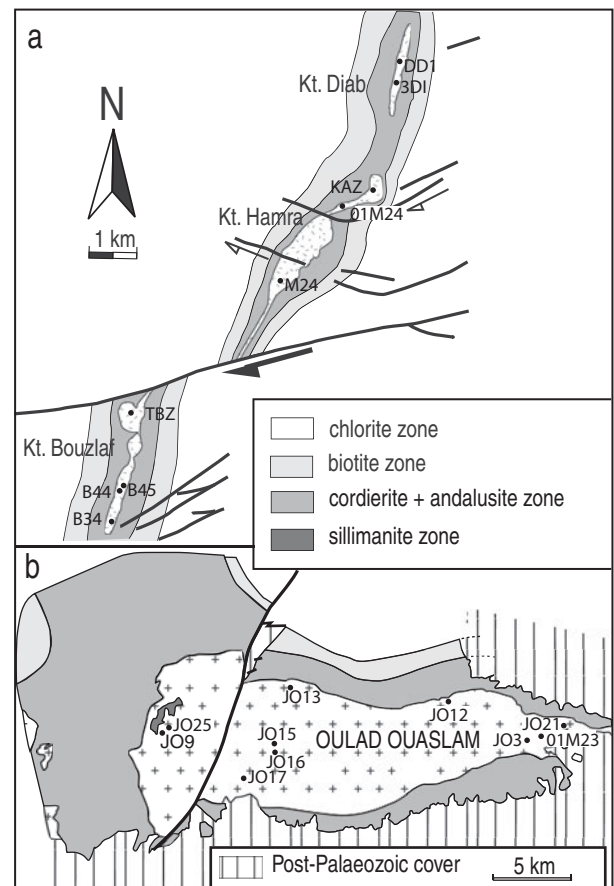


Figure 2. Low-pressure–high-temperature metamorphism around (a) the BHD granophyric microgranites (modified from Essaifi *et al.* 2001) and (b) the eastern Jebilet cordierite-bearing granodioritic pluton (modified from A. Chemesseddoha, unpub. Ph.D. thesis, University of Rennes I, Rennes, 1986). Location of the Sr–Nd samples is indicated. The other samples were collected from Kettara intrusion (GSK, DK13, DK23, DK30, GK3, MK5 and DK25 mafic–ultramafic rocks; MTK and MGTK microgranites), Oled Har intrusion (OH6 and 00M03 gabbros; MOH1 and 00M04 microgranites), El Mna (EM4 gabbro, EM7 quartz-diorite and EM6 microgranite), Jbel Bouzlaf intrusion (BZN3 and MBZN3 microgranites) and central Jebilet pluton (00M01 granodiorite) (see Fig. 1b).

association and the granodioritic plutons. They contain numerous types of enclaves, particularly of the Proterozoic rocks (Huvelin, 1977; Boulton & Gasquet, 1995; Dostal *et al.* 2005) that constitute the basement of the Variscan fold belt of Morocco (Michard, 1976; Piqué *et al.* 1993).

2.b. Geology of the Jebilet Carboniferous magmatism

At the present level of exposure, the bimodal association in the Jebilet massif comprises: (1) mafic–ultramafic plutons (peridotites and gabbros) with alkaline microgranitic stocks and dykes; and (2) volumetrically insignificant intermediate rock types (quartz diorites) found at gabbro/granitoid contacts, which may represent zones of magma mixing. Thin aplitic to perlitic rhyolites and rhyodacitic volcanoclastic rocks are also found in the Sarhlef schists (Bordonaro, Gaillet &

Michard, 1979; Aarab & Beauchamp, 1987). The calc-alkaline granodiorite plutons form two larger plutons.

2.b.1. Bimodal association

The bimodal plutonism (>65% mafic–ultramafic, the remainder is felsic) occurs as numerous felsic and mafic intrusions of some hundreds of metres in thickness and a few kilometres in length (Fig. 1b). They are arranged into three N–S to NE–SW lineaments that are broadly parallel to local shear zones.

The mafic–ultramafic rocks include mafic–ultramafic cumulates (gabbros, peridotites) forming stock or sill-like layered intrusions showing centimetre-scale banding, and dolerite dykes which cut across both the intrusions and the country rocks (Fig. 3a–c). Deformation within these intrusions is very heterogeneous, and subvertical centimetre- to metre-scale shear zones with strong planar fabrics enclose lenticular domains of sub-isotropic gabbros. The Kettara intrusion is a stratified sill composed of a lower banded series of ultramafic cumulates cut by an upper series of mafic cumulates (massive and layered leucogabbros) (Fig. 3a). In the undeformed rocks, magmatic textures are preserved despite an incipient–moderate recrystallization. The magmatic minerals include olivine, clinopyroxene, plagioclase, spinel, ilmenite, apatite and quartz, while minerals related to later alteration include amphibole, chlorite, muscovite, serpentine, epidote, prehnite, anatase and calcite. The cumulate rocks are medium–coarse-grained with ortho- to mesocumulate textures. The ultramafic cumulates are peridotites with olivine and chromian spinel as the cumulus phases and plagioclase, clinopyroxene and ilmenite as the intercumulus phases. The mafic cumulates are leucogabbros with olivine and plagioclase as the cumulus phases while clinopyroxene and ilmenite form the intercumulus phases. Minimum crystallization temperatures for the mafic–ultramafic cumulates were estimated from the clinopyroxene geothermometer (Lindsley & Anderson, 1983) at 1000–1100 °C (Essaifi, 1995). The non-cumulate mafic rocks form gabbros and dolerites with ophitic and subophitic textures, respectively. The gabbros vary from olivine gabbros and ilmenite-rich gabbros to quartz gabbros, while the dolerites range from olivine-bearing to quartz-bearing dolerites (Aarab & Beauchamp, 1987). Mafic–ultramafic cumulates are also present in the majority of the other intrusions of the bimodal association. Mafic–ultramafic rocks crop out in the western part of the the El Mna composite intrusion (Fig. 1b) while intermediate–felsic rocks form the eastern part.

The felsic rocks of the bimodal association crop out as metre-wide dykes enclosing mafic enclaves within the mafic–ultramafic intrusions (Fig. 3d, e) or as stocks within composite mafic–felsic intrusions (e.g. Oled Har, El Mna). They also form elongated and stretched intrusions of more than 10 km in length and less than 700 m wide in a western lineament composed of the Koudiat Bouzlaf, Hamra and Diab intrusions (the BHD

intrusions, Fig. 2a). They consist of microgranitic rocks that contain cross-cutting mafic dykes (synplutonic dolerites; Fig. 3g) and leucocratic microgranular enclaves. These granitoids are locally highly deformed and have been metasomatically altered to gneissic trondhjemites and tonalites (Essaifi *et al.* 2004b). The less-deformed granitoids are observed near the boundaries with country rocks where deformation is heterogeneous. They are monzonitic microgranites that have millimetre-scale phenocrysts in a micrographic–granophyric groundmass showing a weak planar fabric. The primary minerals include quartz, plagioclase, microcline, biotite and amphibole as essential minerals and fluorite, apatite, zircon, ilmenite and allanite as accessory minerals. The phenocrysts are quartz, euhedral plagioclase and aggregates of Cl- and Fe-rich biotite (annite) and blue-green amphibole (hastingsite-ferropargasite). The groundmass is composed of quartz aggregates, plagioclase and microcline showing micrographic and granophyric (spherulitic) associations. Plagioclase phenocrysts in these weakly altered microgranites are sericitized (phengitic muscovite), while biotite is partially replaced by chamosite or by pumpellyite and ilmenite is altered to leucoxene.

Intermediate rocks (quartz-diorites) are present in some composite intrusions where they are localized at the contact between the felsic and the mafic–ultramafic rocks. In these intrusions field evidence, including cross-cutting relationships between intrusions of differing compositions, net veining structures and magma mixing/mingling features, indicates contemporaneous emplacement of the felsic and mafic magmas (Fig. 3f). In the El Mna intrusion (Fig. 1b), the quartz-diorite exhibits a coarse (up to 5 cm) pegmatitic texture and contains plagioclase, amphibole, biotite, K-feldspar, quartz, calcite, chlorite, ilmenite, leucoxene, apatite and zircon. The rock is characterized by abundant (30–40 vol%) centimetre-scale acicular amphibole (ferrohornblende) which is partially or completely replaced by biotite and chlorite, and contains inclusion trails of ilmenite. Plagioclase is present as subhedral crystals altered into calcite and sericite. Biotite can reach 25% of the total rock volume, and some biotite crystals have inclusions of zircon. The groundmass contains quartz that invades K-feldspar (microcline) leading to formation of secondary granophyric associations. Apatite occurs as inclusions in the other phases.

A 330.5 ± 0.68 – 0.83 Ma age was obtained for a microgranitic sample of the BHD intrusions by U–Pb dating of zircon using isotope dilution thermal ionization mass spectrometry (ID-TIMS) (Essaifi *et al.* 2003). The gabbroic rocks have not been dated but, as mentioned above, field evidence demonstrates contemporaneous emplacement of felsic and mafic magmas.

2.b.2. Granodioritic plutons

There are two main cordierite-bearing granodioritic plutons in the area: the eastern and central Jebilet plutons. Within the country rocks, tightening of folds

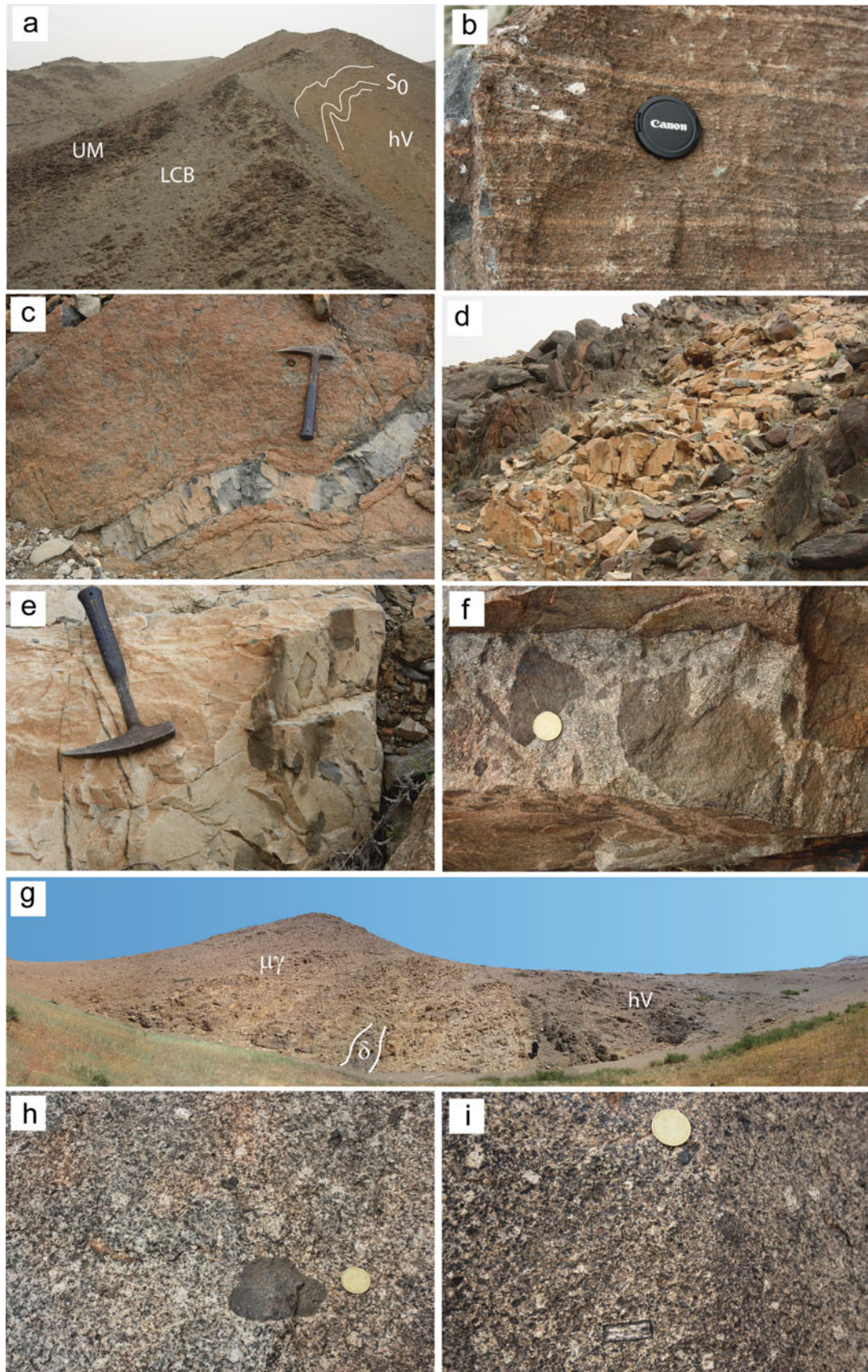


Figure 3. (Colour online) Field photos of the Jebilet magmatism: (a) view within the Kettara mafic–ultramafic layered intrusion showing upper Visean metaturbidites (hV) cropping out in anticline window overlaid by ultramafic cumulates (UM) and leucogabbros (LCB); (b–e) outcrops of the Kettara intrusion showing (b) centimetre-scale layering in the ultramafic cumulates (scale piece is 58 mm across); (c) a rapidly chilled and weakly folded doleritic dyke cross-cutting ultramafic cumulates; (d) a felsic dyke cross-cutting ultramafic cumulates and enclosing mafic enclaves; (e) the mafic enclaves are elongated and occur most abundantly at the intrusive contact, decreasing rapidly towards the centre of the dyke; (f) mafic enclaves within quartz-diorite in the Jbel Bouzlaf intrusion (scale piece is 22 mm across); (g) view showing an E–W cross-section of the Kouadiat Bouzlaf microgranites ($\mu\gamma$) enclosing synplutonic mafic dykes (δ) and intruding upper Visean metaturbidites; and (h, i) outcrops of the cordierite-bearing granodiorite of the eastern Jebilet pluton showing (h) a dark magmatic microgranular enclave and (i) a large xenocryst of andalusite (scale piece is 22 mm across).

in the metamorphic aureole indicates an increase of strain intensity towards the pluton boundaries (Le Corre & Saquaque, 1987; Lagarde, Ait Omar & Roddaz, 1990). In the northern contact aureole of the eastern Jebilet pluton, injection of granitic magma occurs either perpendicular to or along the stratification plane. Within the plutons strain is generally low, and the pre-full-crystallization planar fabric is weak or absent (Boummane & Olivier, 2007), but strain intensity increases towards the pluton margins where a well-defined planar fabric is present and S/C structures are frequent. Ultramytonites are developed in kilometre- to metre-scale shear zones within the plutons. The two plutons are essentially composed of porphyritic biotite±cordierite-bearing granodiorite, but modal compositions range from monzogranites to tonalites (A. Chemesseddoha, unpub. Ph.D. thesis, University of Rennes I, Rennes, 1986; M. K. Ben Salah, unpub. Ph.D. thesis, University Cadi Ayyad, Marrakesh, 1989; El Amrani El Hassani, 1996). The granodiorite is composed of K-feldspar megacrysts (2–3 cm) enclosed in a mesostasis (3–7 mm) of biotite, plagioclase, K-feldspar, cordierite and quartz. Biotite and muscovite±tourmaline-bearing leucogranites are also present at the boundaries between the plutons and the country rock, or as dykes and stocks that cut across the granodiorite. The leucogranites are affected by centimetre-scale shear zones with a mylonitic fabric.

Two types of enclaves are found in the plutons: (1) homogeneously distributed mafic microgranular enclaves with a tonalitic–dioritic composition (Fig. 3h), interpreted as resulting from mingling between a mafic, mantle-derived magma and the granodioritic magma (El Amrani El Hassani, 1996); and (2) aluminous and ferromagnesian xenoliths (made up of aluminosilicates, cordierite, garnet, spinel, biotite and feldspars) present mainly in the eastern Jebilet pluton (Fig. 3i). Hydrothermal alteration is marked in the granodioritic plutons by transformation of biotite into chlorite, K feldspar into muscovite and plagioclase into sericite, while cordierite is altered into pyrophyllite, pinnite and chlorite. The leucogranites are locally affected by extensive alteration leading to total disappearance of feldspar and development of greisens composed of quartz, muscovite and tourmaline.

In the granodioritic plutons Mrini *et al.* (1992) obtained an isochron at 327 ± 4 Ma, an age that was considered to record emplacement. In the leucogranites that cut across the biotite±cordierite granodiorite Mrini *et al.* (1992) obtained an Rb–Sr isochron at 295 ± 15 Ma, consistent with the ages of the other leucogranitic rocks elsewhere in the Western Meseta (e.g. the Oulmes leucogranitic pluton dated at 298 ± 6 Ma (Rb–Sr whole-rock); 296 ± 3 Ma (SHRIMP, U–Pb on zircon) and 308 ± 8 Ma (U–Pb on monazite); Mrini *et al.* 1992; Baudin *et al.* 2001; Fig. 1a).

In summary, both the plutons of the bimodal association and the granodioritic plutons were emplaced in the Jebilet massif at *c.* 330 Ma. Later dykes and stocks of leucogranite were intruded into the granodi-

orite plutons and the country rocks at *c.* 300 Ma. On the basis of Sr and Nd initial isotope ratios at the time of crystallization, the present investigation aims to distinguish the sources of the different rock types and test if mixing between melts from different sources has occurred. In addition, isotope studies on Variscan magmatism in Morocco are rare (Z. Mrini, unpub. Ph.D. thesis, University of Clermont Ferrand, Clermont Ferrand, 1985; Gasquet *et al.* 1992; Mrini *et al.* 1992; Ajaji *et al.* 1998) and this study on the Carboniferous magmatic rocks of the Jebilet massif can be used to place constraints on the genesis of the granitic plutons of the Variscan belt of Morocco.

3. Sampling and analytical methods

Depending on the grain size, samples weighing up to 5 kg were collected to represent the range of rock types exposed and to cover the whole area of the bimodal intrusions. Whole-rock geochemical analyses were carried out on samples taken from the different rock types of the main intrusions within the bimodal association, and used with whole-rock geochemical data on the Jebilet peraluminous granodioritic plutons (El Amrani El Hassani, 1996). For Sr–Nd isotopic studies samples were selected as representative fresh rock, and aim to cover the range of lithological variation within the intrusions. Samples were selected from: (1) mafic–ultramafic rocks of the Kettara mafic–ultramafic intrusion and of the Oled Har, J. Bouzlaf and El Mna composite intrusions; (2) felsic rocks of the BHD microgranitic lineament and the felsic dykes that cut across the Kettara intrusion and felsic–intermediate rocks of the composite intrusions; and (3) cordierite-bearing granodiorites of both the eastern and the western Jebilet plutons. Samples were used with unpublished Sr–Nd isotope data on the granodiorites and leucogranites (Z. Mrini, unpub. Ph.D. thesis, University of Clermont Ferrand, Clermont Ferrand, 1985). The powder samples were prepared using an agate mortar.

Whole-rock chemical analyses were performed at the University of Rennes (France) by X-ray fluorescence spectrometry using a Philips PW 1404 sequential spectrometer. Accuracy for major elements is estimated at 1–3%, except for MnO and P₂O₅ (5%). For trace elements, accuracy is of the order 5% for concentrations lower than 30 ppm and 3% for concentrations higher than 30 ppm. Selected samples were analysed for rare Earth elements by inductively coupled plasma mass spectrometry (ICP-MS) at the Centre de Recherches Pétrographiques et Géochimiques (CRPG), Nancy, France) and at the Laboratoire de Géodynamique des Chaînes Alpines, Grenoble using a VG PQ2+ spectrometer, following the procedures described by Barrat *et al.* (1996). The accuracy is estimated at 5% when chondrite-normalized concentrations are >10 ppm and at 10% when they are lower. These geochemical data are presented in Table 1.

Sr and/or Nd isotopic compositions were analysed in 30 samples (Table 2), including different

Table 1. Major (wt%) and trace element (ppm) data of representative samples from the intrusive rocks of the Jebilet massif (for locations, see Fig. 1b)

| Rock type Sample Location | Ultramafic and mafic cumulates | | | | | | Non cumulative mafic rocks | | | | | |
|---|--------------------------------|-------------------|-------------------|------------------|------------------|------------------|----------------------------|------------------------|------------------|-------------------------|-------------------|-------------------|
| | Prd DK13 KK | Prd DK14 KK | Lcb DK30 KK | Lcb GK2 KK | Lcb GK3 KK | Lcb EM4 EM | Trt GSK KK | μ Gab OH6 OH | Dol BBN JB | μ Gab DK23 KK | Dol BKD BHD | Dol BBS BHD |
| SiO ₂ | 40.07 | 40.78 | 44.98 | 48.07 | 44.72 | 51.14 | 46.98 | 49.99 | 48.79 | 48.09 | 49.77 | 50.38 |
| Al ₂ O ₃ | 7.28 | 7.66 | 21.39 | 19.53 | 19.91 | 18.65 | 14.48 | 15.32 | 15.41 | 15.4 | 14.53 | 14.43 |
| Fe ₂ O ₃ ^a | 9.88 | 9.5 | 7.59 | 4.3 | 5.48 | 7.16 | 9.39 | 10.43 | 10.44 | 10.34 | 11.3 | 11.41 |
| MnO | 0.17 | 0.15 | 0.11 | 0.08 | 0.1 | 0.14 | 0.16 | 0.16 | 0.18 | 0.18 | 0.22 | 0.2 |
| MgO | 28.27 | 28.35 | 8.33 | 8.12 | 10.95 | 5.92 | 11.83 | 7.88 | 7.76 | 9.89 | 7.39 | 7.04 |
| CaO | 5.22 | 4.25 | 11.21 | 15.25 | 11.24 | 10.41 | 11.42 | 11.07 | 10.68 | 10.22 | 10.67 | 10.82 |
| Na ₂ O | 0 | 0 | 1.34 | 1.63 | 1.2 | 2.69 | 1.25 | 2.11 | 2.02 | 1.83 | 1.82 | 2.58 |
| K ₂ O | 0.06 | 0.04 | 0.82 | 0.26 | 1.17 | 0.89 | 0.27 | 0.69 | 1.09 | 0.21 | 1.02 | 0.37 |
| TiO ₂ | 0.4 | 0.49 | 0.55 | 0.36 | 0.5 | 0.94 | 0.78 | 1.54 | 1.4 | 1.34 | 1.31 | 1.35 |
| P ₂ O ₅ | 0.03 | 0.04 | 0.04 | 0.04 | 0.05 | 0.09 | 0.07 | 0.16 | 0.13 | 0.14 | 0.13 | 0.11 |
| LOI | 8.49 | 8.44 | 3.47 | 1.84 | 4.1 | 1.43 | 2.2 | 0.9 | 2.06 | 2.26 | 1.48 | 0.75 |
| Total | 99.87 | 99.7 | 99.83 | 99.48 | 99.42 | 99.46 | 98.83 | 100.24 | 99.96 | 99.9 | 99.64 | 99.44 |
| Nb | 4 | 1 | 1 | 4 | 5 | 7 | 4 | 7 | 5 | 4 | 7 | 7 |
| Zr | 27 | 31 | 37 | 36 | 47 | 84 | 49 | 103 | 90 | 100 | 89 | 88 |
| Y | 6 | 7 | 12 | 6 | 11 | 24 | 20 | 36 | 32 | 29 | 34 | 31 |
| Sr | 15 | 11 | 187 | 212 | 341 | 241 | 67 | 144 | 177 | 158 | 131 | 131 |
| Rb | 6 | 6 | 65 | 21 | 77 | 37 | 19 | 38 | 31 | 12 | 56 | 10 |
| Co | 97 | 97 | 46 | 25 | 41 | 23 | 46 | 41 | 46 | 45 | 39 | 43 |
| V | 89 | 101 | 113 | 107 | 93 | 204 | 212 | 288 | 273 | 259 | 312 | 313 |
| Ni | 1132 | 1386 | 223 | 145 | 358 | 54 | 327 | 107 | 72 | 217 | 40 | 33 |
| Cr | 2002 | 2015 | 264 | 1041.5 | 1018.5 | 414 | 721 | 333 | 303 | 460 | 140 | 115 |
| Ba | 13 | 19 | 36 | 37 | 33 | 101 | 11 | 108 | 222 | 76 | 118 | 322 |
| Ga | 7 | 7 | 14 | 12 | 12 | 18 | 15 | 18 | 17 | 17 | 17 | 18 |
| Cu | 3 | 23 | 66 | 102 | 51 | 17 | – | 29 | 58 | 57 | 11 | 53 |
| Zn | 61 | 62 | 43 | 31 | 43 | 53 | – | 56 | 80 | 77 | 66 | 128 |
| Th | <1 | <1 | 1 | <1 | <1 | 2 | – | 2 | <1 | 2 | <1 | <1 |
| Pb | <1 | <1 | 1 | 1 | 2 | 2 | – | 3 | 5 | <1 | 3 | 9 |
| La | 0.66 | 0.76 | – | 0.77 | 1.32 | – | 1.11 | – | 4.44 | 6.52 | 6.17 | 7.02 |
| Ce | 2.14 | 1.77 | – | 2.35 | 3.87 | – | 3.59 | – | 12.72 | 16.11 | 16.71 | 17.79 |
| Pr | 0.38 | 0.44 | – | 0.41 | 0.65 | – | 0.67 | – | 2.03 | 2.28 | 2.35 | 2.53 |
| Nd | 2.09 | 2.3 | – | 2.31 | 3.39 | – | 3.92 | – | 10.31 | 11.29 | 10.96 | 11.74 |
| Sm | 0.81 | 0.8 | – | 0.86 | 1.16 | – | 1.53 | – | 3.36 | 3.5 | 3.35 | 3.51 |
| Eu | 0.35 | 0.34 | – | 0.42 | 0.52 | – | 0.69 | – | 1.21 | 1.14 | 1.1 | 1.23 |
| Gd | 1.05 | 1.38 | – | 1.18 | 1.5 | – | 2.39 | – | 4.32 | 4.34 | 4.19 | 4.4 |
| Tb | 0.18 | 0.2 | – | 0.21 | 0.26 | – | 0.41 | – | 0.75 | 0.68 | 0.74 | 0.77 |
| Dy | 1.2 | 1.28 | – | 1.44 | 1.83 | – | 2.88 | – | 4.5 | 4.43 | 5.03 | 5.24 |
| Ho | 0.27 | 0.31 | – | 0.3 | 0.38 | – | 0.68 | – | 1.05 | 1.00 | 1.06 | 1.11 |
| Er | 0.71 | 0.85 | – | 0.82 | 1.08 | – | 1.72 | – | 2.93 | 2.81 | 3.02 | 3.19 |
| Yb | 0.75 | 0.81 | – | 0.77 | 1.02 | – | 1.83 | – | 2.75 | 2.59 | 2.88 | 3.05 |
| Lu | 0.11 | 0.15 | – | 0.12 | 0.15 | – | 0.31 | – | 0.42 | 0.4 | 0.45 | 0.47 |
| ASI | 0.76 | 0.99 | 0.91 | 0.64 | 0.84 | 0.77 | 0.63 | 0.63 | 0.64 | 0.71 | 0.62 | 0.59 |
| Mg no. | 0.85 | 0.86 | 0.68 | 0.79 | 0.8 | 0.62 | 0.71 | 0.6 | 0.6 | 0.65 | 0.56 | 0.55 |

rock types of the bimodal association and one clinopyroxene separated from one gabbro as well as two samples from each granodioritic pluton. In addition, Sr isotopes were analysed in three host rock samples (Sarhlef schists) (Essaifi *et al.* 2004a). Sr–Nd isotopic analyses were carried out at the University of Rennes (France) using a Finnigan MAT 262 multicollector mass spectrometer. All measured ⁸⁷Sr/⁸⁶Sr were normalized to ⁸⁶Sr/⁸⁸Sr = 0.1194 and measured relative to NBS 987 Sr Standard = 0.71025. The error of ⁸⁷Sr/⁸⁶Sr, including the statistical error obtained during the mass spectrometer run and other error sources such as instrumental reproducibility, is estimated to be ±0.0003. Nd isotopic ratios were normalized to ¹⁴⁶Nd/¹⁴⁴Nd = 0.7219. Additional Sm–Nd isotopic analyses were performed at Syracuse University (USA) following the procedures described by Samson, Hibbard & Wortman (1995). During the course of this study, the NBS 987 Sr standard yielded

a mean ⁸⁷Sr/⁸⁶Sr of 0.710253 at Rennes University; the ¹⁴³Nd/¹⁴⁴Nd value for the La Jolla standard was 0.511855 at the Syracuse Laboratory and 0.511858 at Rennes University. Even though no samples were run at both laboratories, samples collected from the same intrusion (e.g. MOH1 and 00M04 microgranitic samples or OH6 and 00M03 gabbroic samples) yielded similar results, indicating that the Sm–Nd isotopic data from the two laboratories are in good agreement.

4. Results

4.a. Secondary alteration

The Variscan magmatic rocks of the Jebilet massif underwent the combined effects of hydrothermal alteration and strain (Essaifi *et al.* 2004a, b; Essaifi & Hibti, 2008; M. K. Ben Salah, unpub. Ph.D. thesis, University of Cadi Ayyad, Marrakesh, 1989). Element

Table 1. Continued.

| Rock type Sample Location | Quartz-diorites | | | Microgranites | | | | | | | | |
|---|-----------------|-----------|-------------|---------------|------------|------------|------------|------------|------------|------------|-----------|-------------|
| | Q-D | Q-D | Q-D | μ Gr | μ Gr | TTg | TTg | TTg | μ Gr | TTg | μ Gr | TTg |
| | OH4 OH | EM7 EM | MBZN5 JB | KAZ BHD | TBZ BHD | M23 BHD | B34 BHD | B35 BHD | B45 BHD | DD1 BHD | EM6 EM | MBZN4 JB |
| SiO ₂ | 63.69 | 59.52 | 60.62 | 74.48 | 74.4 | 75.43 | 76.19 | 77.4 | 74.17 | 77.01 | 70.14 | 77.58 |
| Al ₂ O ₃ | 15.39 | 13.11 | 14.55 | 12.39 | 12.33 | 12.52 | 12.29 | 13.15 | 12.32 | 12.65 | 13.09 | 12.9 |
| Fe ₂ O ₃ ^a | 5.09 | 12.11 | 7.22 | 2.92 | 4.18 | 2.87 | 2.01 | 0.59 | 2.77 | 1.25 | 2.45 | 1.41 |
| MnO | 0.07 | 0.17 | 0.11 | 0.04 | 0.03 | 0.04 | 0.03 | 0.02 | 0.04 | 0.02 | 0.05 | 0.03 |
| MgO | 2 | 1.18 | 2.74 | 0.2 | 0.15 | 0.3 | 0.19 | 0.06 | 0.12 | 0.21 | 0.17 | 0.07 |
| CaO | 6.86 | 5.67 | 7.34 | 1.78 | 1.13 | 2.43 | 2.1 | 2.73 | 1.03 | 3.01 | 4.55 | 0.37 |
| Na ₂ O | 4.22 | 3.71 | 4.06 | 2.78 | 3.94 | 3.42 | 3.46 | 3.94 | 2.46 | 3.78 | 4.81 | 6.8 |
| K ₂ O | 0.34 | 0.92 | 0.56 | 3.85 | 2.27 | 1.13 | 1.48 | 0.72 | 4.98 | 0.47 | 0.63 | 0.42 |
| TiO ₂ | 1.1 | 1.52 | 1.13 | 0.22 | 0.25 | 0.23 | 0.21 | 0.25 | 0.25 | 0.22 | 0.51 | 0.17 |
| P ₂ O ₅ | 0.24 | 0.47 | 0.11 | 0.04 | 0.04 | 0.04 | 0.04 | 0.04 | 0.04 | 0.05 | 0.06 | 0.02 |
| LOI | 0.58 | 0.87 | 1.5 | 0.53 | 0.7 | 0.96 | 0.98 | 0.53 | 0.87 | 0.72 | 2.72 | 0.49 |
| Total | 99.59 | 99.25 | 99.94 | 99.23 | 99.42 | 99.37 | 98.98 | 99.43 | 99.05 | 99.39 | 99.18 | 100.26 |
| Nb | 19 | 23 | 10 | 22 | 23 | 20 | 19 | 21 | 22 | 20 | 23 | 17 |
| Zr | 539 | 454 | 216 | 316 | 335 | 315 | 272 | 317 | 343 | 269 | 839 | 241 |
| Y | 70 | 99 | 42 | 105 | 106 | 94 | 89 | 92 | 95 | 81 | 115 | 69 |
| Sr | 283 | 145 | 325 | 170 | 126 | 262 | 256 | 332 | 126 | 290 | 214 | 153 |
| Rb | 16 | 37 | 8 | 103 | 86 | 51 | 46 | 20 | 143 | 22 | 34 | 9 |
| Co | 16 | 21 | 19 | 5 | 9 | 10 | 6 | 1 | 7 | 3 | 6 | 2 |
| V | 139 | <1 | 211 | 0 | 0 | 8 | 7 | 6 | 7 | 5 | <1 | 7 |
| Ni | 16 | 8 | 16 | 3 | 4 | 2 | 2 | 1 | 2 | 1 | 12 | 3 |
| Cr | 54 | 10 | 39 | 11 | 7 | 15 | 8 | 6 | 14 | 19 | 20 | 11 |
| Ba | 139 | 289 | 228 | 930 | 524 | 177 | 468 | 103 | 1083 | 135 | 191 | 155 |
| Ga | 22 | 23 | 22 | 21 | 21 | 21 | 19 | 15 | 20 | 18 | 23 | 21 |
| Cu | 5 | 12 | 10 | 4 | <1 | 3.5 | 2.26 | 1.9 | 2 | 2.1 | 5 | <1 |
| Zn | 27 | 86 | 55 | 34 | 33 | 29 | 22 | 10 | 24 | 13 | 23 | 13 |
| Th | 18 | 18 | 8 | 31 | 30 | 32 | 32 | 33 | 31 | 32 | 27 | 18 |
| Pb | 5 | 13 | 4 | 6 | 2 | 5 | 7 | 4 | 5 | 1 | – | 2 |
| La | – | – | – | – | – | 71.05 | 67.59 | 67.08 | 66.51 | 56.86 | – | 49.44 |
| Ce | – | – | – | – | – | 151.89 | 157.76 | 149.24 | 146.28 | 131.79 | – | 111.75 |
| Pr | – | – | – | – | – | 18.56 | 17.84 | 17.91 | 17.38 | 16.17 | – | 13.64 |
| Nd | – | – | – | – | – | 71.59 | 70.54 | 72.56 | 67.3 | 61.63 | – | 52.88 |
| Sm | – | – | – | – | – | 15.72 | 15.55 | 16.93 | 15.22 | 13.89 | – | 12.45 |
| Eu | – | – | – | – | – | 1.31 | 1.33 | 1.43 | 1.52 | 1.61 | – | 1.03 |
| Gd | – | – | – | – | – | 14.6 | 14.87 | 16.41 | 14.37 | 13.19 | – | 12.03 |
| Tb | – | – | – | – | – | 2.47 | 2.46 | 2.7 | 2.41 | 2.22 | – | 2.06 |
| Dy | – | – | – | – | – | 14.98 | 15.34 | 16.74 | 14.51 | 14.06 | – | 13.09 |
| Ho | – | – | – | – | – | 3.03 | 3.18 | 3.46 | 3.08 | 3.00 | – | 2.64 |
| Er | – | – | – | – | – | 8.56 | 8.89 | 8.1 | 8.51 | 8.25 | – | 7.65 |
| Yb | – | – | – | – | – | 9.3 | 9.25 | 8.86 | 8.61 | 10.49 | – | 8.1 |
| Lu | – | – | – | – | – | 1.42 | 1.43 | 1.39 | 1.31 | 1.52 | – | 1.23 |
| ASI | 0.78 | 0.75 | 0.71 | 1.03 | 1.12 | 1.11 | 1.11 | 1.08 | 1.09 | 1.04 | 0.78 | 1.05 |
| Mg no. | 0.44 | 0.16 | 0.43 | 0.12 | 0.07 | 0.17 | 0.16 | 0.17 | 0.08 | 0.25 | 0.12 | 0.09 |

mobility associated with hydrothermal and deformation processes has resulted in minor geochemical changes in the undeformed rocks comparatively to the deformed rocks, where most major elements, especially Na, K, Ca, Mg and Fe, were mobilized. The large-ion lithophile elements (LILE) such as Rb, Ba, Sr, Zn, Pb and Cu were also mobilized. However, there is no evidence that the high-field-strength elements (HFSE), Ti, P, Th, Zr, Nb and Y, or the REE experienced significant mobility during hydrothermal alteration, except inside the fluid channel ways (shear zones). LILEs and related elements will therefore be avoided for the purposes of petrogenetic discussion.

4.b. The ultramafic–mafic rocks of the bimodal association

The mafic–ultramafic rocks include peridotites, gabbros, leucogabbros and dolerites. The majority of these rocks have clearly formed by cumulate processes, producing igneous layering; some mafic rocks are

however found in dykes which are more likely to represent magmatic compositions. High Mg, Ni, Co and Cr contents characterize the peridotites due to olivine and spinel accumulation, and high Ca and Al contents in leucogabbros are due to plagioclase accumulation (Fig. 4). The non-cumulate rocks display intermediate Al₂O₃ (*c.* 14–15 wt%), MgO (*c.* 6–9 wt%) and CaO (*c.* 8–11 wt%) contents (Table 1). A noticeable silica gap (53–59%) separates the mafic–ultramafic series from the other rock units. The mafic–ultramafic rocks have Mg no. (Mg/Mg+Fe) 0.62–0.86 in the cumulate rocks and 0.53–0.7 in the non-cumulate rocks (Fig. 5a). They show a Fe-enriched trend in the FeO*/MgO versus SiO₂ diagram of Miyashiro (1974) (Fig. 5c) and in FeO* versus FeO*/MgO (Aarab & Beauchamp, 1987). The mafic–ultramafic rocks have lower Nb/Y (<0.67) than alkaline basalts. In the TiO₂ versus Zr/P₂O₅ diagram of Winchester & Floyd (1976) the non-cumulate mafic rocks plot in the tholeiitic field (Fig. 6a), which is consistent with the Nb/Y

Table 1. Continued.

| Rock type Sample Location | Microgranites (cont.) | | | | Granodiorites ^b | | | | Leucogranites ^b | | | |
|---|-----------------------|-------------------|------------------|--------------------|----------------------------|---------------------|----------------------|---------------------|----------------------------|----------------------|----------------------|----------------------|
| | μGr OH1 OH | μGr MOH1 OH | TTg MTK KK | μGr MBZN3 JB | Grd J.1.1 CJP | Grd J.4.7 CJP | Grd J.4.20 CJP | Grd J.2.4 EJP | Grd J.2.24 EJP | Lgr J.4.14 CJP | Lgr J.4.21 EJP | Lgr J.OZ.9 EJP |
| SiO ₂ | 75.57 | 73.77 | 76.19 | 76.09 | 70.26 | 71.07 | 69.44 | 67.89 | 66.86 | 74.7 | 75.99 | 76.34 |
| Al ₂ O ₃ | 13.63 | 13.55 | 12.98 | 12.52 | 13.91 | 14.04 | 14.47 | 15.37 | 16 | 13.37 | 13.12 | 13.01 |
| Fe ₂ O ₃ ^a | 0.82 | 2.77 | 1.5 | 1.6 | 4.71 | 3.6 | 3.79 | 4.18 | 3.71 | 0.72 | 0.86 | 0.56 |
| MnO | 0.01 | 0.03 | 0.02 | 0.02 | 0.05 | 0.06 | 0.06 | 0.05 | 0.07 | 0.21 | 0.01 | 0.02 |
| MgO | 0.36 | 0.39 | 0.51 | 0.11 | 0.81 | 0.8 | 1.06 | 1.33 | 1.3 | 0.21 | 0.18 | 0.07 |
| CaO | 2.76 | 3.02 | 2.99 | 0.88 | 1.36 | 1.58 | 0.92 | 1.75 | 1.73 | 0.43 | 0.34 | 0.37 |
| Na ₂ O | 5.37 | 4.28 | 3.99 | 3.91 | 2.5 | 2.53 | 2.27 | 2.6 | 3.58 | 2.46 | 2.18 | 3.55 |
| K ₂ O | 0.29 | 0.82 | 0.23 | 3.12 | 4.72 | 4.3 | 5.03 | 4.28 | 3.88 | 6.04 | 5.82 | 4.24 |
| TiO ₂ | 0.38 | 0.42 | 0.3 | 0.15 | 0.49 | 0.46 | 0.55 | 0.6 | 0.53 | 0.12 | 0.08 | 0.04 |
| P ₂ O ₅ | 0.21 | 0.25 | 0.07 | 0.01 | 0.13 | 0.15 | 0.15 | 0.19 | 0.18 | – | – | – |
| LOI | 0.43 | 0.47 | 0.43 | 1.24 | 0.95 | 0.57 | 1.29 | 1.01 | 1.25 | 0.81 | 0.49 | 0.77 |
| Total | 99.83 | 99.77 | 99.21 | 99.65 | 99.89 | 99.16 | 99.03 | 99.25 | 99.09 | 99.07 | 99.07 | 98.97 |
| Nb | 18 | 19 | 18 | 19 | – | – | – | – | – | – | – | – |
| Zr | 315 | 313 | 380 | 235 | 134 | 60 | 70 | 48 | 42 | – | – | – |
| Y | 74 | 72 | 95 | 93 | 34 | 23 | 33 | 21 | 21 | – | – | – |
| Sr | 264 | 322 | 379 | 232 | 89 | 81 | 98 | 190 | 450 | 55 | 43 | 127 |
| Rb | 11 | 76 | 15 | 56 | – | – | – | – | – | – | – | – |
| Co | 4 | 10 | 6 | 0.5 | 52 | 56 | 59 | 63 | 53 | 46 | – | 43 |
| V | 19 | 22 | 11 | 9 | 54 | 53 | 63 | 73 | 59 | – | – | – |
| Ni | 5 | 6 | 8 | 3 | 13 | 11 | 12 | 16 | 28 | – | – | – |
| Cr | 39 | 25 | 16 | 6 | 31 | 30 | 38 | 53 | 46 | – | – | – |
| Ba | 105 | 258 | 127 | 1271 | 60 | 370 | 844 | 670 | 815 | 152 | 105 | 168 |
| Ga | 18 | 20 | 17 | 21 | – | – | – | – | – | – | – | – |
| Cu | <1 | 2.9 | – | 4.3 | – | – | – | – | – | – | – | – |
| Zn | 8 | 24 | – | 30 | – | – | – | – | – | – | – | – |
| Th | 19 | 23 | – | 21 | – | – | – | – | – | – | – | – |
| Pb | 5 | 7 | – | 8 | – | – | – | – | – | – | – | – |
| La | 65.91 | 51.43 | – | 65.75 | 39.1 | 34.3 | 35.8 | 39.4 | 28 | – | – | – |
| Ce | 139.73 | 120.58 | – | 132.39 | 86.8 | 71 | 77.2 | 83.6 | 59.7 | – | – | – |
| Pr | 15.91 | 13.85 | – | 16.69 | 9.4 | 7.97 | 8.56 | 9.05 | 6.23 | – | – | – |
| Nd | 60.01 | 54.9 | – | 66.08 | 36.6 | 31.1 | 33.4 | 34.6 | 25.6 | – | – | – |
| Sm | 13.15 | 12.03 | – | 14.93 | 8.33 | 7.26 | 7.36 | 7.33 | 5.6 | – | – | – |
| Eu | 1.15 | 1.17 | – | 1.49 | 0.78 | 0.76 | 1.09 | 1.06 | 1.05 | – | – | – |
| Gd | 12.95 | 12.01 | – | 14.75 | 7.88 | 7.05 | 6.74 | 6.43 | 4.87 | – | – | – |
| Tb | 2.09 | 1.94 | – | 2.33 | – | – | – | – | – | – | – | – |
| Dy | 12.98 | 11.58 | – | 14.61 | 8.05 | 7.93 | 6.18 | 6.19 | 4.47 | – | – | – |
| Ho | 2.59 | 2.3 | – | 3.11 | – | – | – | – | – | – | – | – |
| Er | 7.15 | 6.6 | – | 9.09 | 4.65 | 4.59 | 3.37 | 3.49 | 2.53 | – | – | – |
| Yb | 6.22 | 6.45 | – | 9.1 | 4.45 | 4.47 | 3.2 | 3.35 | 2.42 | – | – | – |
| Lu | 0.85 | 0.94 | – | 1.33 | 0.67 | 0.66 | 0.48 | 0.52 | 0.37 | – | – | – |
| ASI | 0.96 | 1.01 | 1.06 | 1.1 | 1.19 | 1.2 | 1.33 | 1.27 | 1.21 | 1.18 | 1.25 | 1.17 |
| Mg no. | 0.47 | 0.22 | 0.4 | 0.12 | 0.25 | 0.31 | 0.36 | 0.39 | 0.41 | 0.37 | 0.29 | 0.2 |

^aTotal Fe calculated as Fe₂O₃; ^bOriginal data for granodiorites and leucogranites from El Amrani El Hassani (1996).

ASI = molar Al₂O₃/(CaO+Na₂O+K₂O); Mg no. = molar Mg/(Mg+Fe); – not available; Prd – peridotite; Trt – troctolite; Lcb – leucogabbro; Q-D – quartz-diorite; μGab – microgabbro; Dol – dolerite; μGr – granophyric microgranite; TTg – trondhjemitite/tonalite gneiss; Grd – granodiorite; Lgr – leucogranite.

ratios and the Fe-enrichment. The mafic–ultramafic rocks are metaluminous (Fig. 7a). The non-cumulate mafic rocks have higher TiO₂ and Fe₂O₃* contents than the cumulate rocks, and plot within the field of experimental peridotite melts (Fig. 6b).

The mafic–ultramafic rocks have low but variable ΣREE contents (10–62 ppm, 1–10×chondrite), reflecting different abundances and compositions of intercumulus liquids. The lowest concentrations are in the peridotites (ΣREE = 11 ppm) and the highest in the non-cumulate rocks (fringing microgabbros and doleritic dykes, ΣREE = 51–62 ppm), while the leucogabbros have intermediate concentrations (ΣREE = 12–17 ppm). All the mafic–ultramafic rocks display flat ((Gd/Yb)_N = 1.06–1.38) heavy rare Earth elements (HREE) patterns (Fig. 8a). The cumulate rocks have

light rare Earth elements (LREE) depleted ((La/Yb)_N = 0.4–0.9) patterns reflecting dominance of accumulated crystals over interstitial liquids, while the non-cumulate rocks (microgabbros and dolerites) have flat and linear patterns ((La/Yb)_N = 1.1–1.7). Some mafic–ultramafic rocks display a small Eu anomaly, either positive (Eu/Eu* = 0.9–1.2) related to plagioclase accumulation or negative (Eu/Eu* = 0.65–0.9) related to olivine accumulation. All the analysed Jebilet mafic–ultramafic rocks have similar chondrite-normalized HREE patterns, suggesting that they were derived from a common mantle source.

In the primitive mantle-normalized spiderdiagrams (Fig. 8d), the non-cumulate mafic rocks are characterized by flat HFSE patterns and lack the negative Nb anomaly that might be expected in calc-alkaline magmas.

Table 2. Rb, Sr, Sm and Nd concentrations (ppm) and Sr and Nd isotopic ratios of the intrusive rocks of the Jebilet massif

| Sample | Location | Rock type | Rb | Sr | ⁸⁷ Rb/ ⁸⁶ Sr | ⁸⁷ Sr/ ⁸⁶ Sr | ±2σ | (⁸⁷ Sr/ ⁸⁶ Sr) _i | Sm | Nd | ¹⁴⁷ Sm/ ¹⁴⁴ Nd | ¹⁴³ Nd/ ¹⁴⁴ Nd | ±2σ | ε _{Nd(T)} | T _{DM} (Ma) ^a |
|--------|----------|-----------|------------------|------------------|------------------------------------|------------------------------------|-----|--|-------|-------|--------------------------------------|--------------------------------------|-----|--------------------|-----------------------------------|
| GK2 | KK | CPX | 0.37 | 15.88 | 0.067 | 0.704787 | 6 | 0.70448 | 1.33 | 2.65 | 0.3044 | 0.513237 | 8 | 7.2 | ^b |
| GSK | KK | Trt | 20.8 | 65.7 | 0.916 | 0.707867 | 7 | 0.70367 | 1.86 | 4.68 | 0.24 | 0.513178 | 4 | 8.7 | ^b |
| DK13 | KK | Prd | 6.56 | 12.98 | 1.463 | 0.711337 | 8 | 0.70463 | – | – | – | – | – | – | – |
| DK23 | KK | μGab | 12.4 | 149 | 0.241 | 0.707341 | 8 | 0.70624 | 3.56 | 11.9 | 0.1809 | 0.512771 | 4 | 3.3 | ^b |
| DK30 | KK | Lcb | 65 | 187 | 1.006 | 0.711388 | 8 | 0.70666 | 1.08 | 3.25 | 0.2003 | 0.513003 | 9 | 7.0 | ^b |
| GK3 | KK | Lcb | 77.3 | 332.5 | 0.673 | 0.711756 | 8 | 0.70867 | – | – | – | – | – | – | – |
| MK5 | KK | Lcb | 83.5 | 94.8 | 2.55 | 0.717165 | 10 | 0.70547 | – | – | – | – | – | – | – |
| DK25 | KK | Prd | 1.525 | 6.44 | 0.685 | 0.709952 | 9 | 0.70681 | – | – | – | – | – | – | – |
| 00M03 | OH | Gab | – | – | – | – | – | – | 4.97 | 17.1 | 0.1753 | 0.512828 | 7 | 4.6 | ^b |
| OH6 | OH | μGab | 38 | 144 | 0.764 | 0.707836 | 8 | 0.70425 | 4.08 | 13.5 | 0.1833 | 0.512844 | 5 | 4.6 | ^b |
| EM4 | EM | Lcb | 37 | 241 | 0.444 | 0.708887 | 8 | 0.7068 | 2.87 | 10.1 | 0.171 | 0.512712 | 4 | 2.5 | ^b |
| EM7 | EM | Q-D | 37 | 145 | 0.738 | 0.710727 | 9 | 0.70726 | 14.7 | 60 | 0.1482 | 0.512505 | 4 | –0.6 | 1500 |
| B45 | BHD | μGr | 153 | 127 | 3.492 | 0.72556 | 10 | 0.70954 | 14.71 | 65.4 | 0.1361 | 0.512376 | 4 | –2.6 | 1519 |
| 01M24 | BHD | μGr | – | – | – | – | – | – | 14.3 | 64.3 | 0.1344 | 0.512343 | 7 | –3.1 | 1550 |
| KAZ | BHD | μGr | 103 ^c | 170 ^c | 1.75 | 0.71863 | 8 | 0.7106 | – | – | – | – | – | – | – |
| TBZ | BHD | μGr | 86 | 126 | 1.97 | 0.72053 | 8 | 0.71149 | – | – | – | – | – | – | – |
| B34 | BHD | TTg | 49.2 | 268 | 0.532 | 0.713682 | 7 | 0.71124 | 14.7 | 65.47 | 0.1358 | 0.512358 | 4 | –2.9 | 1548 |
| 3DI | BHD | μGr | 88.69 | 124.72 | 2.06 | 0.719472 | 5 | 0.71002 | – | – | – | – | – | – | – |
| B44 | BHD | μGr | 94.7 | 189.6 | 1.446 | 0.71799 | 5 | 0.71136 | – | – | – | – | – | – | – |
| M24 | BHD | μGr | 71.99 | 198.68 | 1.049 | 0.715354 | 9 | 0.71054 | – | – | – | – | – | – | – |
| DD1 | BHD | TTg | 22 | 292.9 | 0.217 | 0.711702 | 6 | 0.71071 | – | – | – | – | – | – | – |
| MOH1 | OH | μGr | 83.8 | 322 | 0.754 | 0.715 | 7 | 0.71154 | 12.43 | 54.77 | 0.1372 | 0.512188 | 4 | –6.3 | 1913 |
| 00M04 | OH | μGr | – | – | – | – | – | – | 11.4 | 50.4 | 0.1372 | 0.512194 | 5 | –6.2 | 1901 |
| EM6 | EM | μGr | 34 | 214 | 0.46 | 0.710066 | 8 | 0.70791 | 17 | 70.2 | 0.1462 | 0.512496 | 4 | –0.6 | 1476 |
| MBZN3 | JB | μGr | 61.5 | 238 | 0.748 | 0.714747 | 8 | 0.71132 | 14.89 | 65.29 | 0.1379 | 0.512474 | 4 | –0.7 | 1359 |
| BZN3 | JB | TTg | 127 | 67 | 5.499 | 0.734452 | 8 | 0.70863 | – | – | – | 0.512505 | 5 | – | – |
| MTK | KK | TTg | 15 | 379 | 0.114 | 0.71238 | 7 | 0.71186 | – | – | – | – | – | – | – |
| MGTK | KK | TTg | 3 | 348 | 0.025 | 0.711856 | 9 | 0.71174 | – | – | – | – | – | – | – |
| 00M01 | CJP | Grd | – | – | – | – | – | – | 7.27 | 32.3 | 0.1359 | 0.512250 | 4 | –4.8 | 1761 |
| 01M23 | EJP | Grd | – | – | – | – | – | – | 7.2 | 35.8 | 0.1215 | 0.512200 | 5 | –5.4 | 1569 |

^aDepleted mantle model age (T_{DM}) calculated following the model of DePaolo (1981a).

^bSamples with ¹⁴⁷Sm/¹⁴⁴Nd > 0.16 do not provide meaningful models.

^cData from Z. Mrini, unpub. Ph.D. thesis, University of Clermont Ferrand, Clermont Ferrand, 1985.

Cpx – clinopyroxene separate from a gabbro; Mmc – mafic magmatic enclave.

Table 2. Continued.

| Sample | Location | Rock type | Rb | Sr | $^{87}\text{Rb}/^{86}\text{Sr}$ | $^{87}\text{Sr}/^{86}\text{Sr}$ | $\pm 2\sigma$ | $(^{87}\text{Sr}/^{86}\text{Sr})_i$ | Sm | Nd | $^{147}\text{Sm}/^{144}\text{Nd}$ | $^{143}\text{Nd}/^{144}\text{Nd}$ | $\pm 2\sigma$ | $\epsilon_{\text{Nd}(t)}$ | T_{DM} (Ma) ^a |
|--------|------------------|-----------|------|------|---------------------------------|---------------------------------|---------------|-------------------------------------|------|-------|-----------------------------------|-----------------------------------|---------------|---------------------------|-----------------------------------|
| JO3 | EJP ^c | Grd | 168 | 307 | 1.58 | 0.71419 | — | 0.7068 | 6.17 | 31.2 | 0.12038 | 0.51219 | — | -5.5 | 1566 |
| JO9 | EJP ^c | Grd | 171 | 175 | 2.85 | 0.72336 | — | 0.71 | 6.85 | 35.8 | 0.11647 | 0.51217 | — | -5.8 | 1535 |
| JO12 | EJP ^c | Grd | 142 | 338 | 1.28 | 0.7123 | — | 0.7063 | 6.41 | 32.99 | 0.11827 | 0.51228 | — | -3.7 | 1389 |
| JO13 | EJP ^c | Grd | 178 | 230 | 2.25 | 0.71863 | — | 0.7081 | 7.53 | 38.48 | 0.11933 | 0.5122 | — | -5.3 | 1533 |
| JO15 | EJP ^c | Grd | 117 | 679 | 0.499 | 0.70637 | — | 0.704 | 2.44 | 13.09 | 0.11346 | 0.51249 | — | 0.6 | 1005 |
| JO16 | EJP ^c | Grd | 110 | 642 | 0.496 | 0.70652 | — | 0.7042 | 2.42 | 12.84 | 0.1147 | 0.51251 | — | 1 | 987 |
| JO21 | EJP ^c | Mme | 67.9 | 318 | 0.618 | 0.7078 | — | 0.7049 | 8.43 | 40.69 | 0.12611 | 0.51242 | — | -1.3 | 1271 |
| JO25 | EJP ^c | Mme | 30.6 | 541 | 0.164 | 0.70494 | — | 0.7042 | 3.19 | 14.23 | 0.13646 | 0.51272 | — | 4.1 | 850 |
| JTa1 | CJP ^c | Grd | 268 | 78.4 | 9.94 | 0.75458 | — | 0.7079 | 8.12 | 38.71 | 0.12759 | 0.51222 | — | -5.2 | 1644 |
| JTa4 | CJP ^c | Grd | 163 | 219 | 2.15 | 0.72058 | — | 0.7105 | 8.29 | 40.15 | 0.12568 | 0.51227 | — | -4.2 | 1523 |
| JBa4 | CJP ^c | Mme | 245 | 89 | 7.98 | 0.74821 | — | 0.7108 | 9.79 | 48.14 | 0.12379 | 0.51223 | — | -4.9 | 1558 |
| JBa5 | CJP ^c | Grd | 301 | 57.5 | 15.3 | 0.77866 | — | 0.707 | 8.37 | 41.85 | 0.12174 | 0.51221 | — | -5.2 | 1557 |
| JBrl | CJP ^c | Grd | 264 | 118 | 6.48 | 0.73876 | — | 0.7076 | 8.61 | 41.87 | 0.12517 | 0.51214 | — | -6.7 | 1736 |
| JO17 | EJP ^c | Lgr | 242 | 54.3 | 13 | 0.77261 | — | 0.7117 | 6.03 | 33.42 | 0.11019 | 0.5121 | — | -7.2 | 1545 |
| JBrs | CJP ^c | Lgr | 259 | 36.4 | 20.7 | 0.80455 | — | 0.7117 | 1.31 | 4.52 | 0.17642 | 0.51235 | — | -4.9 | 3253 |

The cumulate samples generally have lower HFSE and REE contents than the non-cumulates, reflecting the incompatibility of these elements in the main cumulus minerals, and show positive or negative Sr anomalies due to plagioclase accumulation in leucogabbros and olivine accumulation in peridotites, respectively (Fig. 8d). The LILE are generally enriched relative to the REE and HFSE, a feature that can either be related to aqueous fluid involvement (Rollinson, 1993, p. 146) or a characteristic of the source rocks.

The Sr isotopic compositions of the isotropic gabbros, both cumulate and non-cumulate, are variable. Initial $^{87}\text{Sr}/^{86}\text{Sr}$ calculated at 330 Ma lie in the range 0.7037–0.7087, and the intercumulus clinopyroxene measured on a mineral separate has an initial $^{87}\text{Sr}/^{86}\text{Sr}$ ratio of 0.7045 (Table 2). The $^{147}\text{Sm}/^{144}\text{Nd}$ are between 0.17 and 0.3 and the initial $^{143}\text{Nd}/^{144}\text{Nd}$, calculated at 330 Ma, range from 0.51238 to 0.51265 (Table 2). The corresponding $\epsilon_{\text{Nd}(330)}$ values vary from +8.7 to +2.5 (Fig. 9). ϵ_{Nd} generally increases with increasing Mg no. (Fig. 10).

4.c. The microgranites and quartz-diorites of the bimodal association

The microgranites of the bimodal association are highly differentiated with SiO_2 contents ranging from 70 to 80%. The abundances of immobile elements (Th, Nb, P, Zr, Ti, Y and REE) do not fluctuate significantly between samples (Fig. 8e), with low TiO_2 and P_2O_5 contents in the ranges 0.2–0.5% and 0.03–0.06% respectively, except in the Oled Har microgranites where P_2O_5 content reaches 0.25% (Fig. 4). The microgranites have high Zr abundances of between 256 and 380 ppm except in the El Mna composite intrusion where the Zr content reaches 839 ppm (Fig. 4). Nb and Th contents are in the ranges 17–23 ppm and 29–39 ppm respectively, except in the Jbel Bouzlaf composite intrusion where Th content is as low as 17 ppm. Ga and Y contents are in the ranges 15–23 ppm and 57–115 ppm respectively. The least-altered granophyric microgranites, preserved in the outer parts of the BHD intrusions where deformation is heterogeneous, have relatively high K_2O contents (Fig. 5b). They are metaluminous to weakly peraluminous (Fig. 7a) and show characteristics of A-type or ferroan granitoids: (1) petrographically, they contain Fe-rich biotite, hastingsite and fluorite; (2) geochemically, their Mg and Ca contents are low ($\text{MgO} < 0.5\%$, $\text{CaO} < 2\%$), total alkali contents are high (6–8%) and their Fe/Mg ratio is high ($\text{FeO}/(\text{FeO} + \text{MgO}) > 0.8$; Fig. 11a); (3) they have relatively high zircon saturation temperatures (850–900°C, Fig. 7b), similar to temperatures based on zircon typology (850–900°C, Essaifi *et al.* 2003) and on amphibole geothermometry (Holland & Blundy, 1994; Essaifi, 1995). There is no evidence for inherited zircon because separates obtained for previous geochronological studies show euhedral, transparent and colourless magmatic zircons that lack internal structures or visible cores (Essaifi *et al.* 2003). We therefore conclude

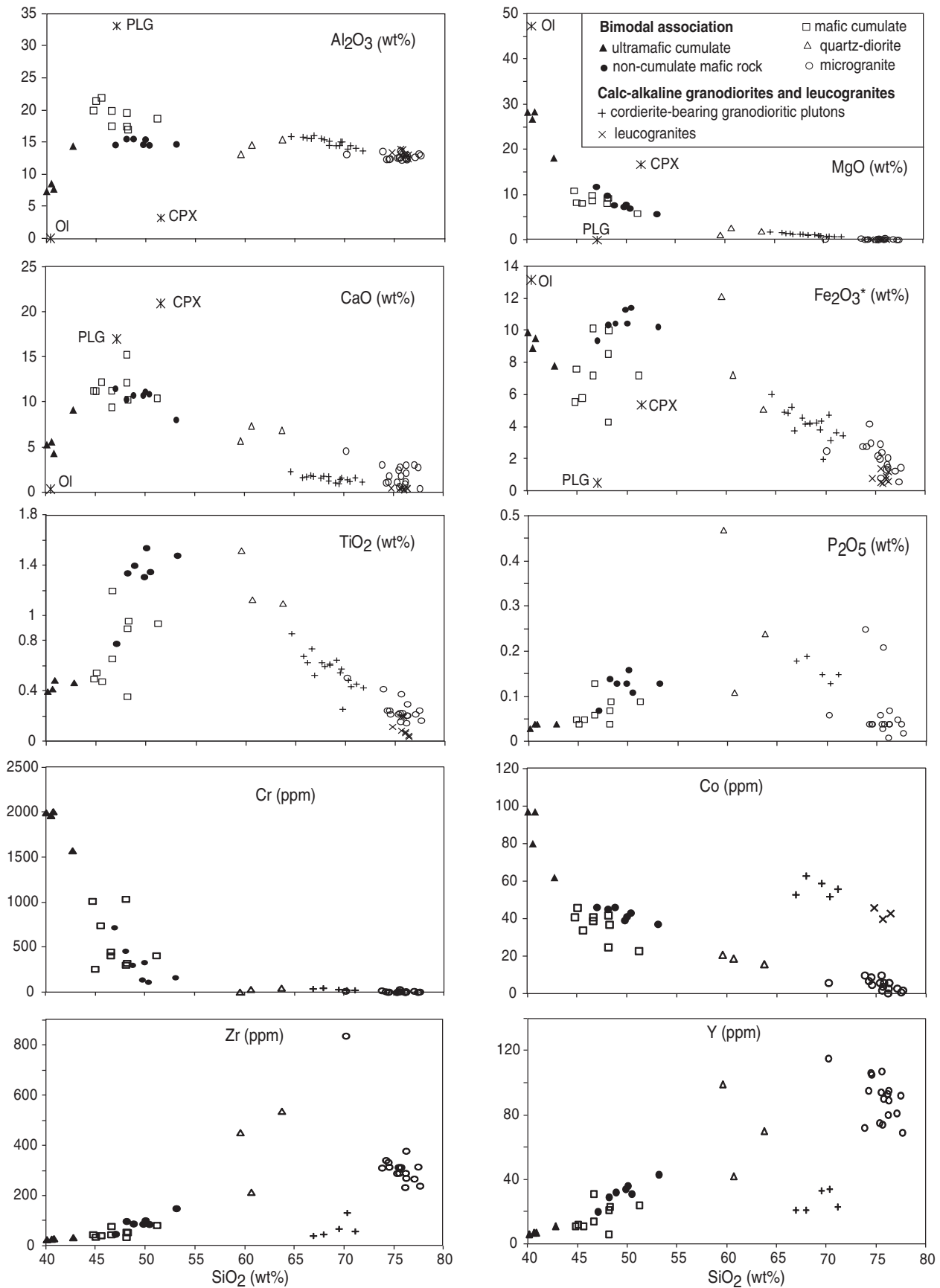


Figure 4. Harker plots for selected major and trace elements of the Jebilet plutonic rocks. CaO, Al₂O₃, MgO and Fe₂O₃* contents of the main fractionating minerals in the mafic–ultramafic cumulates are also plotted. OI – olivine; PLG – plagioclase; CPX – clinopyroxene.

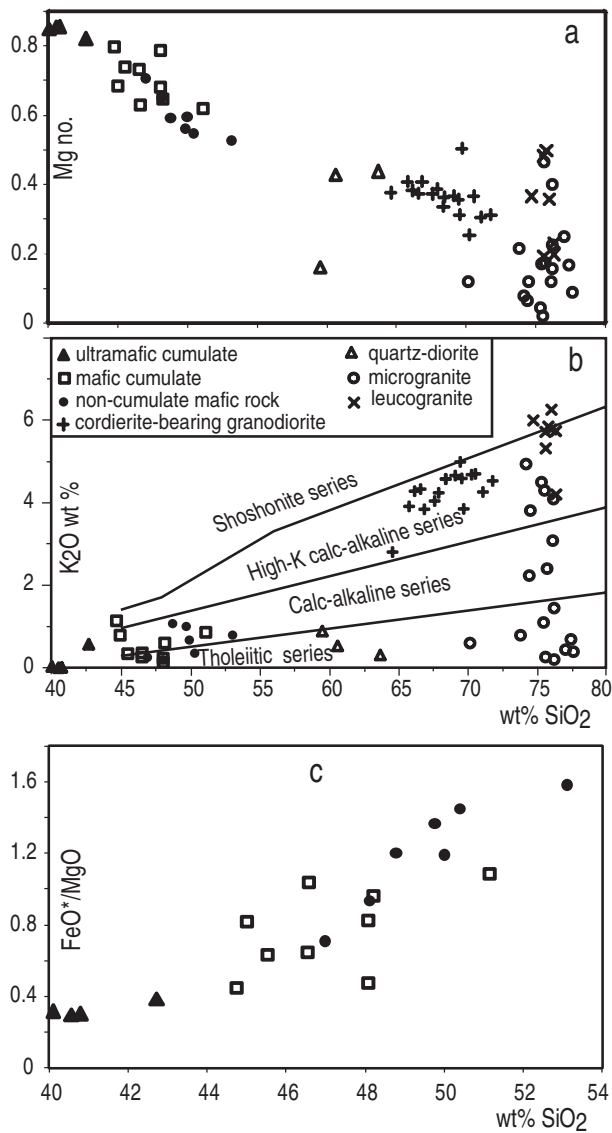


Figure 5. Plot of (a) Mg no. and (b) K_2O versus SiO_2 for the Carboniferous Jebilet intrusive rocks. A silica gap exists between the mafic–ultramafic rocks and the granitoids where the scatter of data points is related to post-magmatic mobilization of K, Mg and/or Fe. The original data for the granodiorites and leucogranites are from El Amrani El Hassani (1996). (c) Plot of the Jebilet mafic–ultramafic rocks in the FeO^*/MgO versus SiO_2 diagram of Miyashiro (1974). Data points show a Fe-enriched trend.

that such temperatures reflect the temperature conditions during melting, indicating that the A-type microgranites represent high-temperature granitic melts. Transformation by loss of K and gain in Na and Ca resulted in moderately high total alkalis in the Jebilet microgranites (Essaifi *et al.* 2004b). The microgranites have relatively high Ga/Al (2.3–3.3) and plot within the A-type compositional field of Whalen, Currie & Chappell (1987), and especially within the A_2 -type granitoid field of Eby (1992) (Fig. 11b, c). This is also confirmed by the classification scheme of Frost *et al.* (2001) using the diagram $FeO^*/(FeO^*+MgO)$ versus SiO_2 (Fig. 11a).

The granophytic microgranites have relatively high REE concentrations ($\Sigma REE = 288\text{--}386$), the concentrations of those in the BHD felsic lineament being identical to those of the felsic rocks of the composite intrusions (Oled Har, El Mna, J. Bouzlaf). They are characterized by uniform patterns (Fig. 8b) with a moderate LREE to HREE fractionation ($(La/Yb)_N = 3.6\text{--}7.1$, $(La/Sm)_N = 2.5\text{--}3.2$), a constant negative Eu anomaly ($Eu/Eu^* = 0.3\text{--}0.4$) and gently sloping HREE chondrite-normalized patterns ($(Gd/Yb)_N = 1\text{--}1.7$). In a primitive mantle-normalized trace element plot, the microgranites show an overall enriched pattern except for depletion in Sr, P, Eu and Ti (Fig. 8e). In addition, Nb shows a significantly negative anomaly relative to the neighbouring elements ($(Nb/La)_N = 0.3\text{--}0.4$).

Chemical compositions of the few intermediate rocks (quartz-diorites) present in the composite intrusions are variable. The SiO_2 content varies between 59 and 69% and $Fe_2O_3^*$ between 5 and 12% (Fig. 4). In the El Mna composite intrusion, evolution from mafic–ultramafic rocks to felsic rocks is accompanied by Fe, Mn and P enrichments in the intermediate rocks (sample EM7, Table 1). Such enrichments are, however, absent from the Oled Har and Jebel Bouzlaf composite intrusions (samples OH4 and MBZN5, respectively). The quartz-diorites have contents of immobile elements similar to those in the felsic rocks, with the exception of Th and Nb contents which are lower and reach 8 and 10 ppm, respectively (sample EM7, Table 1). They have high Zr contents between 216 and 590 ppm (Fig. 4). The ranges of Ga and Y are 21–25 ppm and 42–99 ppm respectively. The quartz-diorites plot in the same alkaline fields as the granophytic microgranites (Fig. 11b, c).

The initial Sr isotopic ratios of the granophytic microgranites of central Jebilet range from 0.7079 (0.7073 in the quartz-diorite of El Mna intrusion) to 0.7119. The $^{147}Sm/^{144}Nd$ are between 0.13 and 0.15 and the initial $^{143}Nd/^{144}Nd$, calculated at 330 Ma, range from 0.51189 to 0.51218. The corresponding $\epsilon_{Nd(330)}$ values vary from -0.6 to -6.3 (Fig. 9). The isotopic range is more restricted when the intrusions are considered separately. $\epsilon_{Nd(330)}$ values are: (1) -6.3 and -6.2 in the microgranites of the Oled Har intrusion; (2) between -2.6 and -3 in the BHD microgranitic intrusions; and (3) -0.6 and -0.7 in the felsic–intermediate rocks of El Mna and Jbel Bouzlaf composite intrusions. These results reveal a spatial variation in the microgranites characterized by an increase in the $\epsilon_{Nd(330)}$ values westwards.

4.d. The cordierite-bearing granodiorites and associated leucogranites

The cordierite-bearing granodiorites form differentiated products of a calc-alkaline plutonic suite (Fig. 5b). The plutons also include monzogranites and tonalitic to dioritic magmatic enclaves (El Amrani El Hassani, 1996; Gasquet, Stussi & Nachit, 1996). They have intermediate to acidic compositions ($SiO_2 = 64\text{--}76\%$),

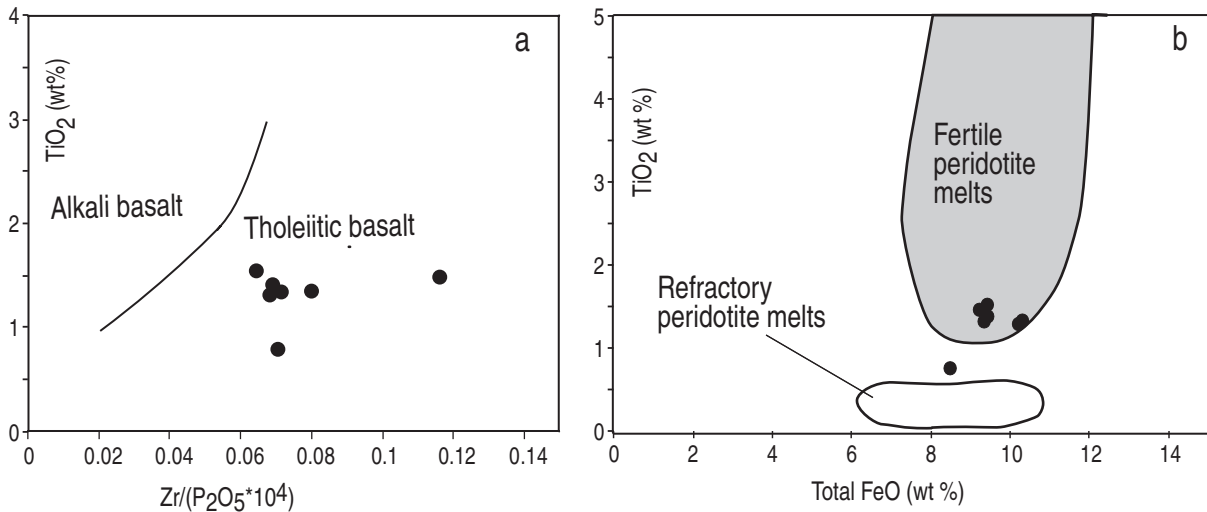


Figure 6. (a) Plot of TiO_2 versus $\text{Zr}/\text{P}_2\text{O}_5$ for non-cumulate mafic rocks of the Jebilet bimodal intrusive rocks. (b) Total Fe_2O_3 versus TiO_2 diagram for the non-cumulate mafic rocks compared with fields for experimental peridotite melts (Falloon *et al.* 1988).

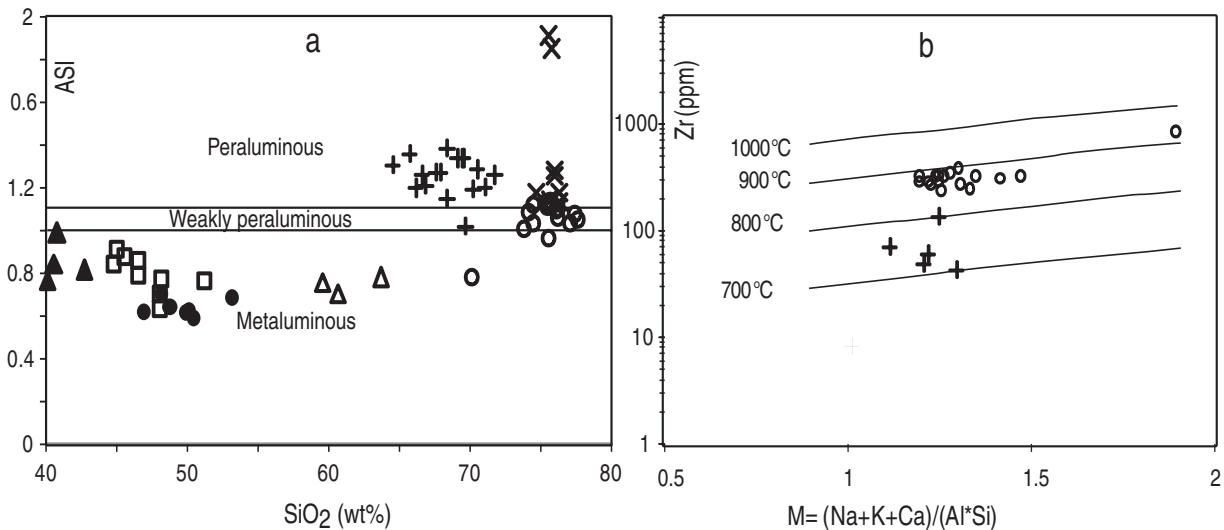


Figure 7. (a) SiO_2 versus ASI (molar $\text{Al}_2\text{O}_3/(\text{CaO}+\text{Na}_2\text{O}+\text{K}_2\text{O})$) index; and (b) cation ratio $(\text{Na}+\text{K}+2\text{Ca})/(\text{Al}^*\text{Si})$ versus Zr diagram (after Watson & Harrison, 1983). Symbols as in Figure 4. The original data for the granodiorites are from El Amrani El Hassani (1996).

the most differentiated pluton being the central Jebilet granodiorite. They form continuous and regular trends, distinct from those of the microgranites (Fig. 4). Their biotite compositions correspond to those of calc-alkaline granitic magmas (El Amrani El Hassani, 1996; Gasquet, Stussi & Nachit, 1996), but the systematic presence of magmatic cordierite in the plutons indicates the peraluminous character of the magma, which is also indicated by $A/\text{CNK} > 1$ (Fig. 7a) and a normative corundum content of 1.7–3.2% (El Amrani El Hassani, 1996; Gasquet, Stussi & Nachit, 1996).

The cordierite-bearing granodioritic plutons show significant negative anomalies in Sr, Zr and Ti (Fig. 8f) and moderate negative anomalies in P and Eu. They have relatively low zircon saturation temperatures (700–800 °C, Fig. 7b), similar to temperatures based on

zircon typology and biotite geothermometry (El Amrani El Hassani, 1996). They have intermediate REE abundances (144–207 ppm); the contents in the central Jebilet pluton are identical to those of the eastern Jebilet pluton (El Amrani El Hassani, 1996). They are characterized by uniform REE patterns (Fig. 8c) with a slight to moderate LREE to HREE fractionation ($(\text{La}/\text{Yb})_N = 4.56\text{--}6.98$, $(\text{La}/\text{Sm})_N = 2.93\text{--}3.34$), a moderate negative Eu anomaly ($\text{Eu}/\text{Eu}^* = 0.32\text{--}0.66$) and flat to gently sloping HREE chondrite-normalized patterns ($(\text{Gd}/\text{Yb})_N = 0.97\text{--}1.29$). The leucogranites that cut across the granodiorites are highly differentiated ($75 < \text{SiO}_2 < 79\%$) and strongly peraluminous ($A/\text{CNK} > 1$, Fig. 7a). They have very low contents of CaO (<0.5%), Fe_2O_3^* (<1.3%) and MgO (<0.2%) and higher Co contents than the microgranites (Fig. 4).

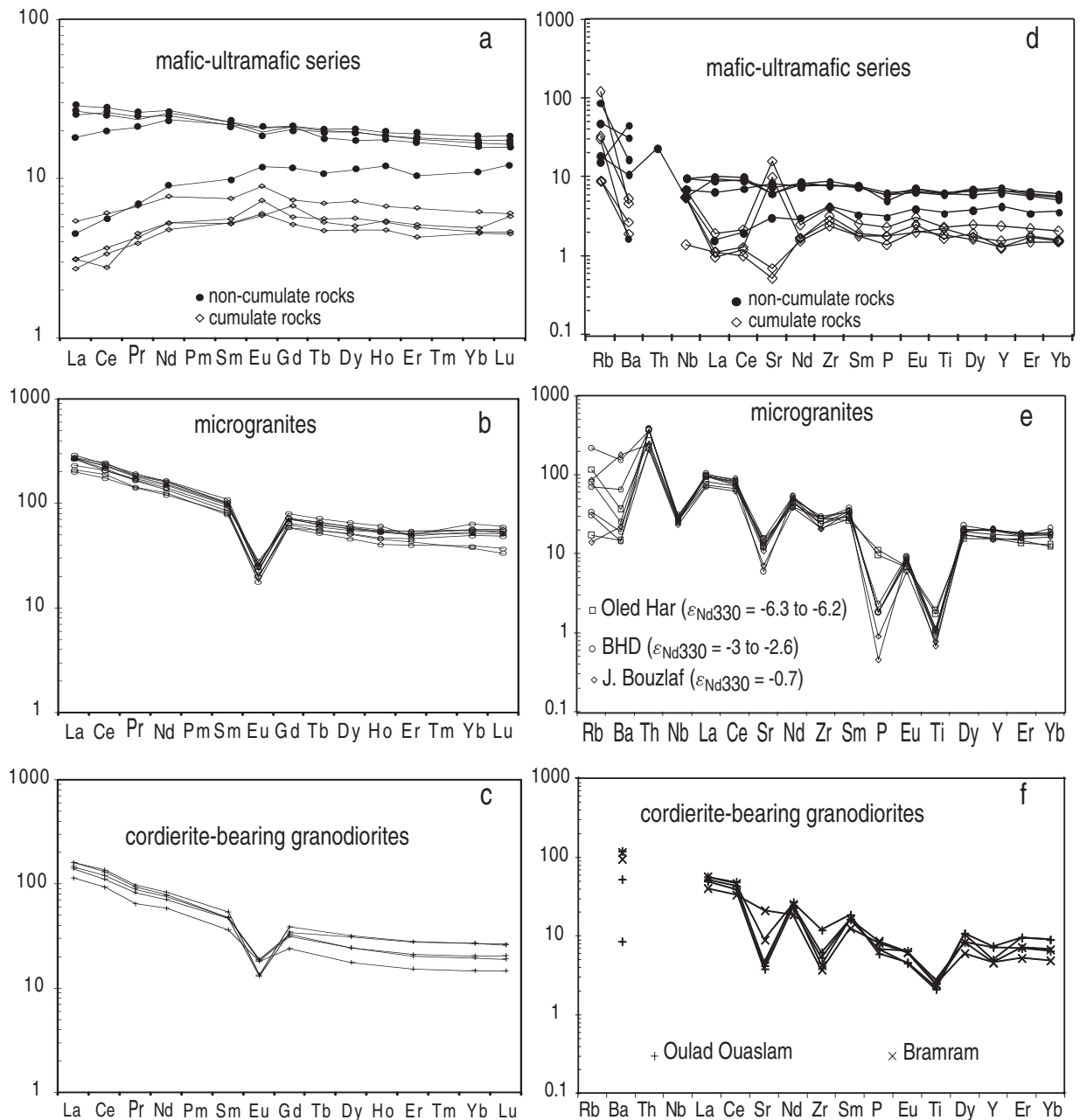


Figure 8. Chondrite-normalized REE plot for representative rocks of the Jebilet magmatism: (a) mafic-ultramafic rocks; (b) granophyric microgranites; and (c) cordierite-bearing granodiorites. Normalizing values are from Evensen, Hamilton & O'Nions (1978). Primitive mantle-normalized trace element diagrams for representative rocks of the Jebilet magmatism: (d) mafic-ultramafic rocks; (e) granophyric microgranites ($\epsilon_{\text{Nd}330}$ values of the microgranites in the corresponding intrusions are indicated); and (f) cordierite-bearing granodiorites. Normalizing values are from Sun & McDonough (1989). The original data for the granodiorites and leucogranites are from El Amrani El Hassani (1996).

In the granodioritic plutons and their magmatic enclaves, the initial Sr isotopic ratios, calculated at 330 Ma, vary largely in the range 0.704–0.7108 while the initial Nd isotopic ratios range from 0.51186 to 0.51242 (Table 2). The corresponding $\epsilon_{\text{Nd}(330)}$ values vary from –6.7 to –4.8 in the cordierite-bearing granodiorites, while an $\epsilon_{\text{Nd}(330)}$ of +4.1 is found in a mafic microgranular enclave of dioritic composition (Fig. 9). The leucogranites have the highest initial $^{87}\text{Sr}/^{86}\text{Sr}$ isotopic ratios (0.7117–0.7177) and low $\epsilon_{\text{Nd}(300)}$ values with the lowest $\epsilon_{\text{Nd}(300)}$ value

(–7.2) observed in the Jebilet Carboniferous magmatic rocks.

4.e. The host schist series

The country rocks of the Jebilet magmatism are predominantly metapelites derived from middle–upper Viséan shales deposited in anoxic platform (Beauchamp, 1984) and are affected by a very-low- to low-grade metamorphism contemporaneous with a post-Viséan shortening (Huvelin, 1977). Their

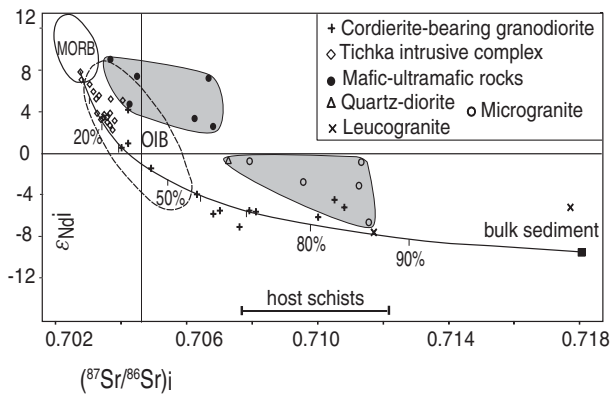


Figure 9. Initial $^{87}\text{Sr}/^{86}\text{Sr}$ versus initial ϵ_{Nd} values of the Jebilet plutonic rocks. The granitoids of the Tichka plutonic complex are also plotted. A mixing curve between the mafic end-member deduced for the Tichka plutonic complex (Gasquet *et al.* 1992) ($(^{87}\text{Sr}/^{86}\text{Sr})_i = 0.7027$, Sr = 700 ppm, Nd = 20 ppm, $\epsilon_{\text{Nd},i} = +7.6$) and a bulk-sediment corresponding to the mean composition of the protolith from which most of the granites in Morocco were derived ($(^{87}\text{Sr}/^{86}\text{Sr})_i = 0.718$, $\epsilon_{\text{Nd},i} = -9$, Sr = 150 ppm, Nd = 30 ppm) is shown. The bar represents $(^{87}\text{Sr}/^{86}\text{Sr})_{330}$ of the country rocks. Also shown are the fields of MORB and OIB (Wilson, 1989). The original data for the Jebilet granodiorites and leucogranites are from Z. Mrini (unpub. Ph.D. thesis, University of Clermont Ferrand, Clermont Ferrand, 1985) and data for the Tichka plutonic complex are from Gasquet *et al.* (1992).

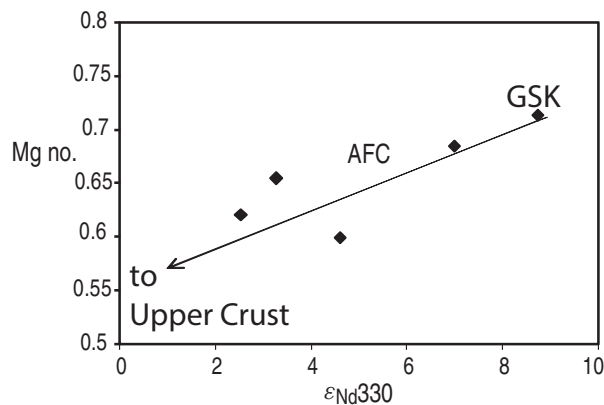


Figure 10. Mg no. (as a differentiation index) versus $\epsilon_{\text{Nd}(330)}$ in the Jebilet mafic-ultramafic rocks. The observed evolutionary trend (arrow) is consistent with mixing or assimilation and fractional crystallization (AFC) processes between a mafic end-member represented by GSK sample (Mg no. = 7 and $\epsilon_{\text{Nd}(330)} = +8.7$) and an upper crustal end-member (bulk-sediment with Mg no. = 4 and $\epsilon_{\text{Nd}(330)} = -9$).

geochemical data suggest derivation from a continental magmatic arc (Moreno *et al.* 2008). In the spiderdiagram of Figure 12, a representative sample of Sarhlef schists collected by composite sampling is compared to greywackes from passive-margin settings and active-margin settings, after Floyd (1991). A negative Sr anomaly, a positive V, Cr and Ni anomaly, a negative Ta-Nb anomaly and slight enrichments in Ti, Yb and LREE are observed in the Sarhlef schists relatively to the upper crust. There is a general correspondence to the continental arc and active-margin tectonic environ-

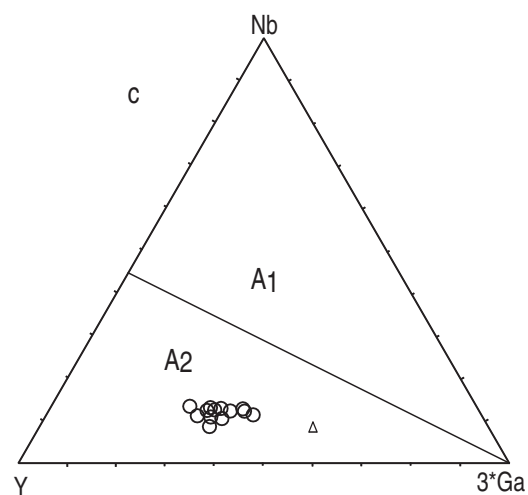
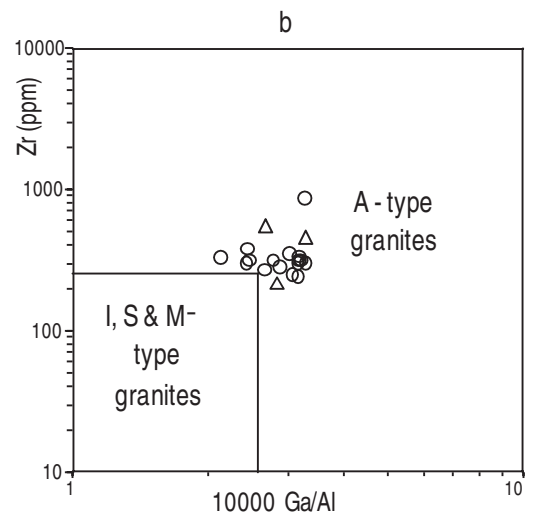
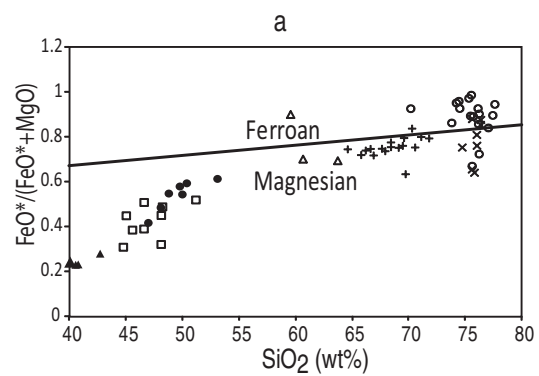


Figure 11. Plots of the (a) Jebilet intrusives in the classification diagram of Frost *et al.* (2001) and (b) Jebilet microgranites (circles) and quartz-diorites (triangles) in the Zr versus 10000 Ga/Al diagram of Whalen *et al.* (1987), showing affiliation with A-type granites. (c) Nb-Y-Ga ternary diagram for the subdivision into A₁- and A₂-type granites (Eby, 1992). Symbols as for Figure 4.

ment, but the presence of a negative Sr anomaly is similar to the passive-margin setting. Sr isotope analysis has been conducted on three samples collected by composite sampling (Essaifi *et al.* 2004a). Their $^{87}\text{Sr}/^{86}\text{Sr}$

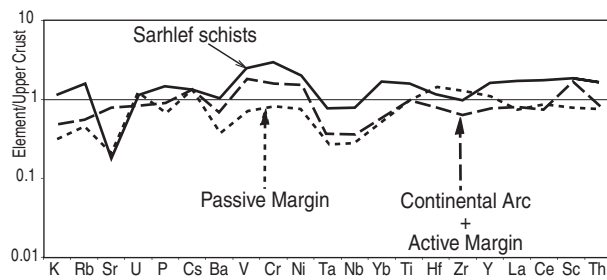


Figure 12. Trace-element concentrations of the Sarhlef schists normalized to upper crustal values (Taylor & McLennan, 1995) and compared to expected patterns of sediments in active-margin and passive-margin settings, after Floyd (1991) and unpublished data (Essaifi).

values at the time of intrusion of the bimodal magmatic association and the granodioritic plutons (330 Ma) vary between 0.7077 and 0.7121 (Fig. 9).

5. Discussion

5.a. Potential magmatic processes

In situ fractional crystallization (FC) clearly played a major role in the development of the ultramafic–mafic rocks as indicated by mineral layering, cumulate textures and major and trace element geochemistry (e.g. Eu anomalies). However, field relationships, geochemistry and Sr and Nd isotopic compositions allow us to recognize that other petrogenetic processes, such as crustal assimilation, magma mixing and hydrothermal alteration, were also operative in the formation of the Jebilet plutons.

Field relationships provide evidence for magma mixing and mingling (dioritic zones and enclaves in the plutons), incorporation of crustal material (crustal xenoliths in the granodiorites) and metasomatic alteration. As far as possible, samples for geochemical and isotopic analysis were selected from areas that were not affected by significant metasomatism (therefore preserving a record of other petrogenetic processes). If fractional crystallization was the dominant process by which these magmas evolved, little change would be expected in some incompatible element ratios (e.g. La/Nb, Zr/Nb) or in isotopic ratios across the igneous suite. The wide variation in these ratios clearly indicates that magmas were derived from more than one source.

The Carboniferous Jebilet magmatic rocks show large variations in both initial Sr isotopic ratios and ϵ_{Nd} values, which display a broad inverse correlation in the ϵ_{Nd} versus Sr_i space (Fig. 9). Since the whole-rock Sm–Nd system is more resistant to late-stage low-grade perturbations than the Rb–Sr system, this indicates that the scatter of whole-rock Rb–Sr data is not solely related to post-magmatic perturbations but reflects complex petrogenesis. In the mafic–ultramafic rocks, increasing degrees of differentiation (monitored by the Mg no., Fig. 10) are associated with increas-

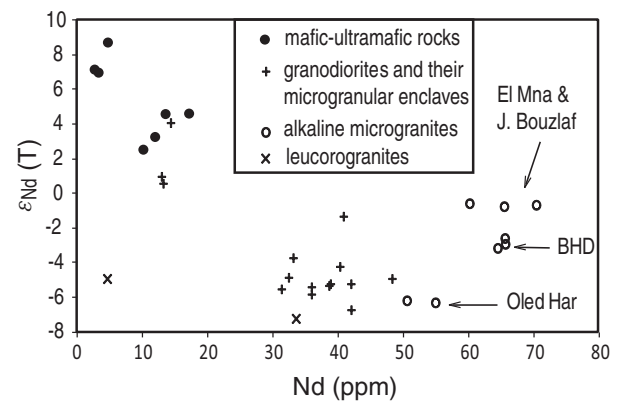


Figure 13. (a) Plot of initial ϵ_{Nd} values versus Nd concentrations.

ing amounts of crustal components (lower ϵ_{Nd} values with decreasing Mg no.). Such a trend is consistent with mixing between mantle-derived and crust-derived magmas or an assimilation and fractional crystallization (AFC) process (DePaolo, 1981b). In the granodioritic samples and the mafic rocks there is a negative correlation between Yb contents and the size of the Eu anomaly, indicating that feldspar fractionation contributes to the size of the negative Eu anomaly in the mafic rocks and the granodiorites. There is however no correlation of Yb contents with the size of the negative Eu anomaly in the microgranites. The Eu anomaly in the microgranites is therefore not due to fractional crystallization of feldspar but is more likely a feature of the source rocks in which plagioclase was partly a residual phase.

Contamination of the microgranites during ascent and emplacement seems probable since they share the same initial isotopic ratios with the host schists (0.707–0.712). Simple contamination is however unlikely in the light of the Nd concentration. The microgranites have higher Nd concentrations (50.4–65.47 ppm) than the metasedimentary rocks (14.4–41.5 ppm; Belkabar *et al.* 2008; Essaifi, unpublished data) and the granodiorites and leucogranites (4.52–48.14 ppm) (Fig. 13). Simple contamination would require that the host schists provide an unacceptably high amount of the bulk Nd. In simple crustal assimilation models, the size of Nb anomaly and concentration of elements most affected by contamination (Ba, Rb, K, LREE, Sr; Thompson *et al.* 1982) are expected to increase with progressively more negative $\epsilon_{Nd(T)}$ values. These relationships are not observed among the microgranites (Fig. 8e). The Nb negative anomaly in the microgranites is therefore difficult to explain by AFC processes; rather it is a characteristic of the source rocks, similar to that of subduction-related magmas. Xenoliths and xenocrysts from the country rocks are widespread in the granodioritic plutons but are absent from the A-type microgranites, suggesting that chemical exchanges between the microgranites and country rocks are of limited extent. Furthermore, preservation of the different Nd isotopic signatures in the different microgranitic intrusions implies that different batches

of magma were produced from different sources or mixtures of different sources. It is therefore suggested that distribution of data points in Figure 13 originates through mixing of different end-members rather than by simple contamination processes. Such end-members are discussed in more detail in the following.

5.b. Inferences on mantle and crustal sources

The mafic–ultramafic rocks have the most primitive isotopic signatures with the lowest $(^{87}\text{Sr}/^{86}\text{Sr})_i$ and highest $\epsilon_{\text{Nd},i}$ values (Fig. 9), whereas the leucogranites and some microgranites are most evolved with the highest $(^{87}\text{Sr}/^{86}\text{Sr})_i$ and lowest $\epsilon_{\text{Nd},i}$ values. The other microgranites and the quartz-diorites on the one hand and the granodiorites and their microgranular enclaves on the other form an intermediate group between the mafic–ultramafic rocks and the leucogranites, suggesting a hybrid origin.

5.b.1. Origin of the mafic–ultramafic rocks

Despite their large variations, the available initial ϵ_{Nd} values (+8.7 to +2.5) and initial $^{87}\text{Sr}/^{86}\text{Sr}$ ratios (0.7037 to 0.7087) support a mantle-derived origin for the mafic–ultramafic series. Although many mantle reservoirs have been proposed (e.g. Rollinson, 1993, p. 233), major possible sources are the subcontinental lithospheric mantle, the mantle wedge above a subduction zone or the asthenospheric mantle. Some fine-grained mafic rocks forming dykes or chilled margins in some of the intrusions may be considered to represent near-liquid compositions. These mafic rocks have consistent, flat trace element and REE patterns, in contrast to the cumulate samples which have more variable trace element compositions. However, even these rocks have rather variable isotopic compositions, suggesting that they have fractionated from slightly or significantly different batches of basic magma. The composition of the source region and parent magma of the mafic–ultramafic series can be approached from the least-contaminated samples in terms of Sr–Nd isotopes. The GSK sample is a fine-grained troctolite dyke that has the most primitive isotopic signature currently recorded in the Jebilet massif ($\epsilon_{\text{Nd},i} = +8.7$, $(^{87}\text{Sr}/^{86}\text{Sr})_i = 0.7037$, Nd = 4.68 ppm, Sr = 65 ppm). This rapidly chilled dyke may represent a melt with a pristine asthenospheric mantle heritage and hence furnish a reliable estimate of the Sr and Nd isotopic composition of the mantle-derived suite. Its high Mg no. (0.7) and MgO as well as compatible element contents suggest that it represents a primary or near-primary melt. This is consistent with the flat to LREE depleted patterns of the non-cumulate mafic rocks (Fig. 8a), patterns that are similar to those of normalized mid-ocean ridge basalt (N-MORB). These non-cumulate rocks have high TiO_2 contents and plot within the field defined by experimental melts of fertile peridotites (Fig. 6b), suggesting that they were most probably derived from fertile asthenosphere. Instrumental neutron activation

analysis (F. Kharbouch, unpub. Ph.D. thesis, University of Bretagne occidentale, Brest, 1994) has however revealed that some mafic rocks of the bimodal association display geochemical features, implying that the asthenospheric mantle was affected by subduction processes. These rocks are relatively enriched in LILE and depleted in HFSE with Nb–Ta negative anomalies. Their Nb/U (14–56) and Th/U ratios (1.9–5.19) can be lower than those of MORB and ocean island basalt (OIB). Such geochemical features cannot be attributed solely to crustal contamination because Th/U ratios of crustal rocks are high (c. 5.0) and crustal assimilation will elevate Th/U ratios higher than those of MORB (c. 3.0) and OIB (c. 3.4) (Jiang *et al.* 2009). Th/U ratios of the slab-released hydrous fluid are low because U, relatively to Th, is preferentially transported in the aqueous fluid from the subducted slab to the mantle wedge (Keppler, 1996; Ayers, 1998). Based on immobile-discrimination diagrams such as the Th–Hf–Ta diagram of Wood (1980), the Jebilet mafic rocks include both MORB-like and destructive plate-margin-like basaltic compositions (Fig. 14a). Such a coexistence of MORB-like and arc-like tholeiitic basalts has also been described in other bimodal associations involving A_2 -type rhyolites and tholeiitic basalts (e.g. the Topsails igneous suite in the Newfoundland Appalachians, Whalen *et al.* 2006). For this reason we believe that, although contamination has played a role in modifying their composition, mafic rocks of the Jebilet massif are thought to be derived from different mantle sources: a depleted MORB mantle and a mantle wedge above a subduction zone.

Gasquet *et al.* (1992) showed that mafic rocks (gabbros and diorites) from the nearby Variscan Tichka plutonic complex (Fig. 1a) are derived from an upper mantle source, and that this high-temperature magma provided the heat for the production of granitoid magmas by partial melting of the continental crust. On the Nd–Sr isotope diagram (Fig. 9), the Tichka plutonic rocks plot within the mantle array as defined by uncontaminated oceanic basalts, whereas most of the Jebilet mafic rocks plot to the right of this field. Clearly the Nd–Sr isotope data of the Jebilet mafic rocks could be accounted for simply by partial melting of a depleted asthenospheric mantle wedge (MORB source mantle) enriched in radiogenic Sr by slab-derived fluids. The fact that Th/Yb ratios are displaced towards higher values in the Th/Yb versus Ta/Yb diagram (Fig. 14b) provides strong evidence for involvement of such slab-derived fluids in the genesis of the Jebilet mafic rocks.

5.b.2. Origin of the microgranites

The Jebilet granophyric microgranites show geological and geochemical features that are characteristic of A-type or ferroan granites (according to criteria proposed by several authors e.g. Collins *et al.* 1982; Whalen, Currie & Chappell, 1987; Eby, 1992; Frost *et al.* 2001): (1) they were intruded to very high levels in the crust as indicated by granophyric intergrowths along with

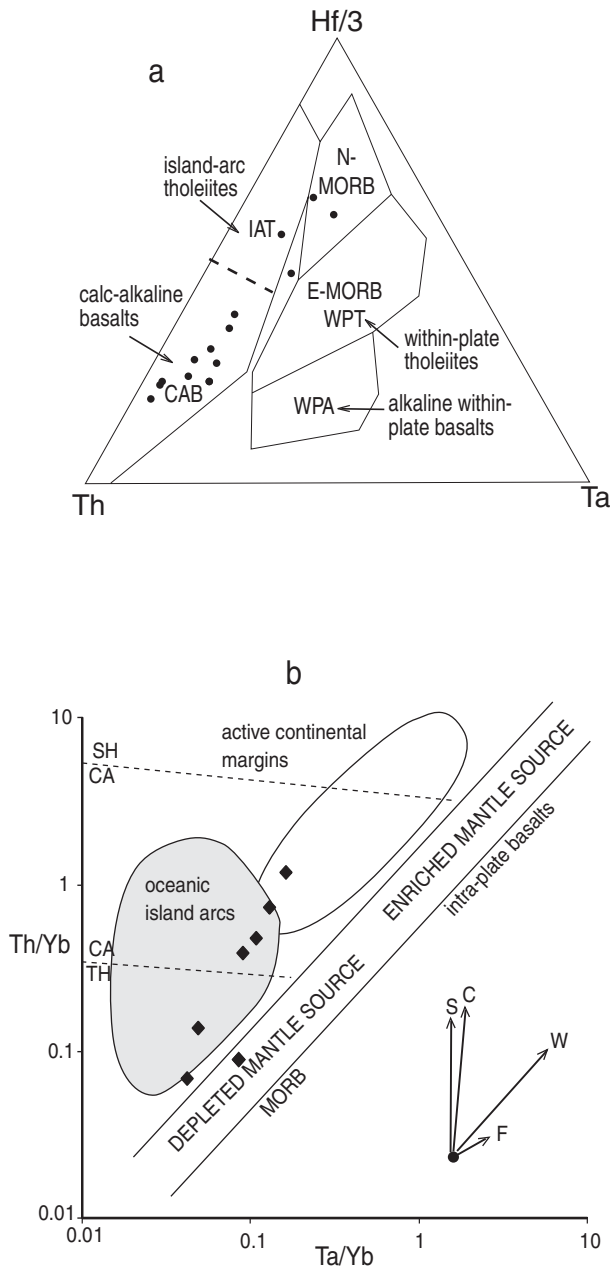


Figure 14. (a) Distribution of the Jebilet mafic rocks in the Th–Hf–Ta discrimination diagram of Wood (1980). (b) Plot of Th/Yb versus Ta/Yb. Vectors shown indicate the influence of subduction components (S), within-plate enrichment (W), crustal contamination (C) and fractional crystallization (F). Dashed lines separate the boundaries of the tholeiitic (TH), calc-alkaline (CA) and shoshonitic (SH) fields (after Pearce, 1983). Original data from F. Kharbouch, unpub. Ph.D. thesis, University of Bretagne Occidentale, Brest, 1994. The mafic rocks of Table 1 are also included in (a) considering the ratios Nb/Ta = 16 and Zr/Hf = 39.

comagmatic subvolcanics emplaced at the same structural level; (2) they contain interstitial Fe and Cl-rich biotite, hastingsite and fluorite; (3) their Mg and Ca contents are low and their REE (except Eu) and HFSE contents are high (Fig. 8b, e); and (4) they have high magmatic temperatures (up to 900 °C, Fig. 7b) and their Fe/Mg and Ga/Al ratios are high (Fig. 11a, b). High Rb/Nb and Y/Nb ratios (Fig. 11c) further suggest that

these granites belong to the A₂ group of Eby (1992), a group of alkaline granitoids derived from continental crust or underplated crust that has been through a cycle of continent–continent collision or the waning stages of arc magmatism (whereas the A₁-type granites emplaced in continental rifts or during intraplate magmatism and represent differentiates of magmas derived from OIB-like sources) (Eby, 1992).

The A-type magmas are regarded as differentiation products of mantle-derived melts through extensive fractional crystallization (e.g. Turner, Foden & Morrisson, 1992; Bonin, 1996; Litvinovsky *et al.* 2002; Mushkin *et al.* 2003) or as partial melts of specific crustal protoliths, either: a granulitic residue from which a granitic melt was previously extracted (Collins *et al.* 1982; Clemens, 1986; Whalen, Currie & Chappell, 1987; Creaser, Price & Wormald, 1991); a charnockitic rock (Landenberger & Collins, 1996); a hornblende-bearing granitoid (Patiño Douce, 1997); or a granulitic metasedimentary rock (Huang *et al.* 2011). They could also result from hybridization between anatectic granitic and mantle-derived mafic magmas (Bédard, 1990; Kerr & Fryer, 1993; Mingram *et al.* 2000; Yang *et al.* 2006), coupled with fractionation processes (Barker *et al.* 1975; Wickham *et al.* 1996).

The presence of a ‘Daly gap’ between mafic–ultramafic rocks and the microgranites and some crust-like geochemical and isotopic features argues against a simple magma differentiation model. Th concentrations in the Jebilet microgranites (20–40 ppm; Table 1) are higher than in the oceanic plagiogranites (Th < 5 ppm; Pearce, Harris & Tindle, 1984), suggesting that these microgranites do not result from the differentiation of the penecontemporaneous tholeiitic basalts (Th ≤ 2 ppm). For the same SiO₂ content, the microgranites of Central Jebilet are especially poor in Ti and Fe compared to the granophyres associated with well-known layered tholeiitic intrusions (e.g. McBirney, 1989; Turner, Foden & Morrisson, 1992). In any case, the Sr initial isotopic ratios and the ε_{Nd} values of the granophyric microgranites are distinct from those of the associated gabbroic rocks (Fig. 9) and leave no doubt that the microgranites did not form simply by extensive fractional crystallization from the coeval mantle-derived mafic magmas. Their origin should therefore involve continental crust, either lower or upper crust.

High REE contents but moderate ε_{Nd(330)} values imply that the sources are not strongly evolved and preclude the derivation of the A-type microgranites from granulitic metasedimentary rocks. The high HREE (Yb > 6.22 ppm, up to 10.5 ppm) and Y (> 69 ppm, up to 115 ppm) contents and flat to gently sloping HREE patterns (Fig. 8b) of the Jebilet microgranites preclude garnet as a residual phase, which implies low pressure (< 7 kbar, Patiño Douce, 1997). Based on comparisons with experimentally produced melts from a variety of crustal lithologies (Holloway & Burnham, 1972; Helz, 1976; Spulber & Rutherford, 1983; Beard & Lofgren, 1991; Skjerlie & Johnston, 1993; Patiño

Douce, 1997), tonalitic sources are found to be the most consistent with observed compositions of these granophyric microgranites. Melting experiments of Patiño Douce (1997) demonstrated that dehydration melting of hornblende-bearing granitoids in the shallow crust ($P \leq 4$ kbar, at depths of 15 km or less) is a likely origin for high-silica metaluminous A-type granites. At 4 kbar and a melt fraction of 20–40%, plagioclase and clinopyroxene are the dominant residual phases of dehydration melting of hornblende-bearing granitoids (Patiño Douce, 1997). Good matches between the composition of the microgranites and the experimentally produced melts from tonalitic sources support a crustal anatexis origin.

The Jebilet granophyric microgranites have Proterozoic depleted-mantle model ages (T_{DM} c. 1.91–1.36 Ga), suggesting that an older crustal component exists in these Carboniferous granitoids. Such old crust, which crops out under the Palaeozoic cover in the Anti-Atlas inliers and is recognized by gravity data under the Palaeozoic formations of the Jebilet massif (Bernardin *et al.* 1988), has been dated in granulitic enclaves of the Triassic lamprophyre dykes that cross-cut the Jebilet massif (Dostal *et al.* 2005) and in the nearby Rehamna massif (Baudin *et al.* 2002). The microgranitic samples from the Oled Har intrusion have the lowest ϵ_{Nd} value (–6.3) of the microgranites. Their T_{DM} ages (c. 1.9 Ga) point to the Eburnean basement (c. 2 Ga) while the other microgranites have lower T_{DM} ages (1350–1550 Ma) that seemingly require a mafic or juvenile (mantle) component. The coeval association of the microgranites with mafic magmas and the presence of net-veining structures and mafic enclaves within the microgranites suggest interaction between felsic and mafic magmas. In the ϵ_{Nd} versus Sr_i space (Fig. 9), the microgranites are characterized by higher initial $^{187}Sr/^{186}Sr$ ratios and lower initial ϵ_{Nd} values than the mafic rocks. Their field appears to extrapolate back to that of the associated mafic rocks, suggesting some form of mixing process, but this broad inverse correlation cannot be fitted by a single curve diagnostic of a simple two-component mixing. The microgranites trend could represent a variable degree of mixing between a mantle source variably enriched by slab-derived fluids and partial melts of the Eburnean metamorphic basement. This is consistent with the fact that the microgranites show an increase in the mantle contribution from east to west, suggesting the existence of independent reservoirs in which magma batches evolved independently by fractional crystallization and magma mixing processes.

Curved evolutions for some elements (Ti, Fe, P, V, Zr) in the bimodal association indicate that mineral fractionation was a main petrogenetic process (Fig. 4). Such evolutions are observed in the El Mna intrusion where the quartz-diorite and the microgranite have a same initial ϵ_{Nd} value (–0.6), consistent with fractional crystallization. The ϵ_{Nd} value (+2.5) of the associated mafic rock requires assimilation of continental crust in order to produce the Nd isotopic composition of

the quartz-diorite and microgranite. The chemical and Sr–Nd isotopic compositions of some microgranites can therefore be explained by a complex petrogenetic process combining fractional crystallization and magma mixing between mantle-derived magmas and crust-derived magmas (represented by the Oled Har microgranites). The differences in the isotopic compositions of the microgranites can be related to the heterogeneity of the mantle sources and to variable degrees of crustal and mantle contribution.

5.b.3. Origin of the granodiorites and leucogranites

The Jebilet granodioritic plutons are emplaced at high structural levels, they contain biotite, cordierite and ilmenite and are strongly peraluminous. They can therefore be attributed to the S-type granite group of Chappell & White (1974). Such granites are largely produced by partial melting of metasedimentary rocks. Barbarin (1996) has distinguished two groups among the S-type granites: (1) biotite-rich, cordierite-bearing granitoids (CPG-type) and (2) muscovite-bearing granitoids (MPG-type). The CPG granitoids are suggested to be produced by ‘dry’ anatexis of crustal rocks enhanced by underplating or injection of hot mantle-derived magmas, which can be preserved as microgranular mafic enclaves within the CPG (Barbarin, 1996). As the Jebilet granodioritic plutons contain numerous microgranular mafic enclaves, they can be attributed to the CPG type.

The T_{DM} ages of the granodioritic plutons (1.76–0.85 Ga) require a Proterozoic source rock. Their strongly peraluminous signature suggests that the source rocks were mainly metasedimentary rocks rather than meta-igneous rocks. However, the plutons display large variations in Sr–Nd isotopic compositions that may indicate the presence of a mantle-derived component, and the granodiorite plutons contain numerous microgranular mafic enclaves. As suggested by Barbarin (1996), these rocks might therefore be derived from anatexis of crustal rocks induced by underplating or injection of hot mantle-derived magmas. The granodioritic plutons have intermediate HREE (2.42 ppm $< Yb < 4.47$ ppm) and Y (21–34 ppm) contents and overall display flat to gently sloping HREE patterns ($(Gd/Yb)_N = 1–1.7$). Fractionation among the HREE, a common feature of S-type granites (e.g. Bernard-Griffiths *et al.* 1985), would indicate the presence of garnet in the residual source, but this feature is lacking in the cordierite-bearing granodiorites of the Jebilet. These magmas were therefore more likely produced by relatively low-temperature (c. 750 °C) anatexis of pelitic sources induced by injection of basalt magmas in the shallow crust. The produced crustal melts underwent hybridization with the coeval basalt magmas and assimilation of pelitic metasediments during ascent of the magmas in the crust. The process of wall-rock assimilation was documented in the Jebilet granodioritic plutons by the occurrence of inherited metamorphic cordierites (which are partly digested

pelitic xenoliths), picked up at 750 °C and 3.5 kbar by the ascending magma (Bouloton, 1992), and therefore representing relics of the assimilated rocks (Fourcade *et al.* 2001). The large variation in the initial Sr isotopic ratios (0.704–0.7108) and the $\epsilon_{\text{Nd}(330)}$ values (–6.7 to +4.1) in the granodioritic plutons indicates isotopic heterogeneity that results from mixing between crust-derived and mantle-derived magmas (Mrini *et al.* 1992) and wall-rock assimilation. The granodiorites define continuous and regular trends in major and trace element diagrams (Fig. 4). In the ϵ_{Nd} versus Sr_i diagram (Fig. 9) the granodiorites and their microgranular enclaves scatter around a hyperbolic mixing curve between a crustal end-member, corresponding to the mean composition of the protolith from which most of the granites in Morocco were derived (Z. Mrini, unpub. Ph.D. thesis, University of Clermont Ferrand, Clermont Ferrand, 1985), and the mantle end-member of the Tichka plutonic complex.

The two mica-leucogranites are strongly peraluminous and can be described as S-type granites of Chappell & White (1974) and muscovite-bearing granitoids (MPG-type) (Barbarin, 1996). The initial Sr isotopic ratio (0.7177) and the $\epsilon_{\text{Nd}(330)}$ value (–7.2) of the Jebilet leucogranites are consistent with direct derivation from crustal sources with a major contribution of aluminous metasedimentary rocks.

5.c. Magma generation/tectonic implications

The question of the heat source required for crustal melting during granitoid genesis is a long-debated topic, with (1) purely crustal mechanisms involving crustal thickening and total heat supply by decay of radioactive elements (e.g. England & Thompson, 1986) and (2) mantle–crust mechanisms involving heat input from the mantle into the crust in various geodynamic situations, such as asthenospheric upwelling (hot spots or extension zones), arc genesis and lithospheric delamination or slab break-off in orogenic zones (e.g. Harris, Pearce & Tindle, 1986; Bussy, Hernandez & von Raumer, 2000; Whalen *et al.* 2006).

The spatial and temporal association of mafic magmatism with alkaline and calc-alkaline felsic magmatism in the Jebilet massif argues for mafic magma-driven partial melting. Among the geodynamic settings where the mantle is classically implicated, hot spots or extension zones can be ruled out on the basis of regional tectonics. Relationships between deformation, magmatism and metamorphism indicate that emplacement of the granodioritic plutons and the bimodal plutonism in the Jebilet massif, as well as emplacement of the wider Carboniferous plutonic suite in the Moroccan Meseta, was contemporaneous with a syntectonic low-pressure regional metamorphism and development of ubiquitous, upright axial plane cleavages, unambiguously indicating horizontal shortening at the orogenic scale (Lagarde, Ait Omar & Roddaz, 1990). Models involving local lithospheric extension in strike-slip-induced basins (e.g. Mitjaviła, Marti & Soriano, 1997;

Essaifi *et al.* 2003) are also not sustainable because the lithospheric thinning required to induce asthenospheric melting is much too great to be a result of strike-slip shearing during plate convergence. In central Jebilet, syntectonic emplacement of magmatic intrusions is consistent with the regional strain pattern that involves NE–SW extension (Fig. 1b), parallel to the southern prolongation of the western Meseta shear zone (Piqué, Jeannette & Michard, 1980; Lagarde & Michard, 1986). The NE–SW extension is accompanied by lateral extrusion of the central Jebilet block and by synconvergence exhumation of the Proterozoic basement and intermediate *P–T* metamorphic rocks in the Rehamna massif (Aghzer & Arenas, 1998; Baudin *et al.* 2001). Such an orogen-parallel extension with exhumation is intimately related to continental collision and occurs even during the early stages of convergence (Seyferth & Henk, 2004).

The Jebilet Carboniferous magmatic rocks were emplaced at *c.* 330 Ma into slightly older upper Viséan (350–333 Ma) marine syntectonic ‘flysch’ metasediments. The positive V–Cr–Ni–Ti anomalies observed in these sediments (Fig. 12) are indicative of a mafic input involving oceanic crust, possibly obducted onto the continent during a collision event (Floyd, 1991; Totten, Hanan & Weaver, 2000). Their spiderdiagram, with a general correspondence to the continental arc and active-margin tectonic environment and the presence of a negative Sr anomaly similar to the passive-margin setting, is best described by mixing between a dominant passive-margin source and a sediment from an active margin setting (Totten, Hanan & Weaver, 2000). In Central Morocco, Carboniferous syntectonic flysch and catastrophic sediments were deposited in a compressional retro-foreland basin where interbedded basaltic lavas, doleritic dykes and gabbro sills were emplaced during thrusting (Ben Abbou *et al.* 2001; Roddaz *et al.* 2002). In the Guemassa massif at the southern prolongation of the Jebilet massif (Fig. 1), basaltic dykes and rhyolites were also emplaced during thrusting. The Moroccan Variscan crust therefore seems to have thickened by extensive sedimentation, volcanism and minor intrusion in the upper crust, with synchronous magmatic underplating and ductile deformation at depth. Such crustal thickening characterizes subduction-related orogens (Lamb *et al.* 1997).

In this context one possible extrusive equivalent of the bimodal association of Central Jebilet is the bimodal basalt-subalkaline/peralkaline rhyolite province of the Southern British Caledonides which is also associated with polymetallic sulphide mineralization (Leat *et al.* 1986; Eby, 1992; Thorpe *et al.* 1993). This association was emplaced within a shallow marine environment in a tectonic setting associated with closure of the Lower Palaeozoic Iapetus Ocean, cessation of oceanic subduction and development of strike-slip tectonism. Because the Moroccan Hercynides are thought to be related to continental subduction (Lagarde, 1989; Piqué & Michard, 1989; Piqué *et al.* 1993; Roddaz *et al.* 2002), the bimodal association of central Jebilet can be

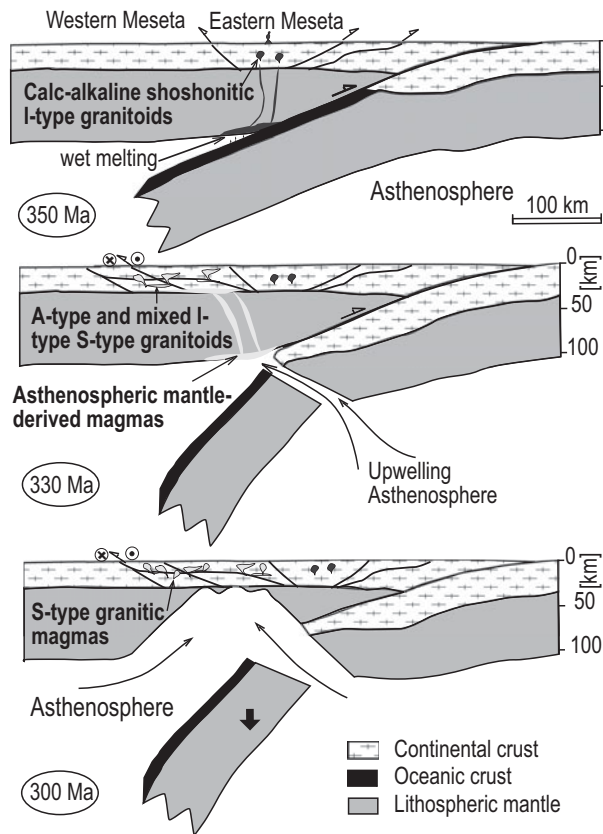


Figure 15. Cartoons showing crust–mantle interaction and subsequent melting and intrusion of Carboniferous granitic and gabbroic intrusions of the Moroccan Mesetas. (a) Westward subduction, partial melting of the lithospheric mantle and generation of potassic–shoshonitic granitic intrusions in the eastern Meseta at *c.* 350 Ma. (b) Cessation of subduction at *c.* 330 Ma, synconvergence extension and exhumation of intermediate *P–T* metamorphic rocks, upwelling of asthenospheric melts, convective removal of the lithospheric mantle, partial melting in the shallow crust and generation of coeval A-type granitic magmas and cordierite-bearing granodioritic plutons. (c) Progressive replacement of the lithosphere by the asthenosphere, leading to generation of leucogranites of purely crustal origin at *c.* 300 Ma.

interpreted as resulting from cessation of continental subduction and development of strike-slip tectonism during collision (Fig. 15).

Possible models leading to the generation of mafic magmas and crustal melting in collisional orogens include slab break-off (e.g. Davies & von Blanckenburg, 1995), convective lithospheric erosion (Houseman, McKenzie & Molnar, 1981) and large-scale delamination of the lithosphere (e.g. Nelson, 1992). Taking into account the evolution of magmatism in the Jebilet massif as well as in the Moroccan Meseta (Mrini *et al.* 1992; El Hadi *et al.* 2006) from calc-alkaline granitoids and mafic magmas of mixed origin to leucogranites of a purely crustal origin and synchronous emplacement of these magmas with regional deformation, convective lithospheric erosion during crustal thickening (Loosveld & Etheridge, 1990) seems more consistent with geochemical and Sr–Nd isotopic constraints. Convective thinning/erosion of the lithospheric mantle induces partial melting of subduction-metasomatized

subcontinental lithospheric mantle, producing early potassic magmas and progressing to intra-plate depleted asthenospheric melts over time (Mahéo *et al.* 2002). Potassic to shoshonitic calc-alkaline I-type granitoids crop out in the eastern Moroccan Meseta where they post-date an early Eo-Variscan folding phase. According to Ajaji *et al.* (1998), the Tanncherfi intrusive complex, emplaced at 344 ± 6 Ma, was derived from mantle sources enriched in LILE and LREE by a subduction process. The evolution from continental lithospheric mantle signature in the Tanncherfi intrusive complex to the asthenospheric signature in the Jebilet massif, as well as in the Tazekka and Tichka massifs (Gasquet *et al.* 1992; Chalot-Prat, 1995), reflects a lithosphere being progressively heated from below (Houseman, McKenzie & Molnar, 1981; Nelson, 1992). Progressive replacement of the lithosphere by the asthenosphere results in elevated Moho temperatures and thus favours crustal melting at sequentially shallower levels (Fig. 15). The calc-alkaline granitoids become increasingly crustally contaminated and are succeeded by partial crustal melts (Turner *et al.* 1999; Wang *et al.* 2004). According to structural, geochemical and Sr–Nd isotopic data, erosion of the mantle lithosphere (thinning) was initiated during crustal thickening and the induced thermal anomaly was responsible for both magmatism and metamorphism in the Variscan Moroccan Meseta.

6. Conclusion

In the Jebilet massif, the post-Viséan crustal shortening was accompanied by an orogen-parallel extension, lithospheric thinning, mantle uplift and progressive melting of the depleted mantle, which produced basaltic magmas. These basalts ascended into the continental crust, including the upper crust, where they formed crustal magma chambers. Temperature elevation due to mantle uplift and basalt emplacement induced crustal anatexis. High-temperature (*c.* 900 °C) melting of tonalitic sources produced A₂-type granitoids, while at low temperatures (*c.* 750 °C) anatexis of metasediments produced cordierite-bearing granitoids. During this evolution, contamination/mixing occurred between mantle-derived magmas and crustal melts, contributing to the large variations of $\epsilon_{\text{Nd}(330)}$ and $(^{87}\text{Sr}/^{86}\text{Sr})_i$ values observed in both the cordierite-bearing granitoids and the A₂-type microgranites. Further contamination occurred by assimilation of country rocks during ascent of the magmas to high crustal levels.

The Jebilet magmatism is an example of granitoid magma production in a complex tectonic setting where plate convergence interacts with a deep process, promoting mantle and crust activation. Structural, geochemical and Sr–Nd isotopic constraints argue for convective thinning/erosion of the lithospheric mantle during thickening. The thermal anomaly induced by the convective thinning of the mantle lithosphere is likely to have brought the heat energy that caused melting of the underlying asthenosphere and coeval production of

calc-alkaline and alkaline granitoids, followed by the production of leucogranites.

Acknowledgements. Constructive comments and suggestions by M. Fowler and another anonymous reviewer greatly improved the presentation of data and the discussion; these comments are highly appreciated, although some wishes could unfortunately not be fulfilled. We wish to thank J. A. Barrat and G. Gruau from Geosciences Rennes for providing some of the Sr–Nd isotope and REE data used in this study. Sm–Nd isotopes were analysed at Syracuse University during post-doctoral research funded by the Fulbright program. We thank S. Fourcade for a review of an early version of this paper. This work represents a contribution to the project URAC 43.

References

- AARAB, E. M. & BEAUCHAMP, J. 1987. Le magmatisme carbonifère pré-orogénique des Jebilet centrales (Maroc). Précisions pétrographiques et sédimentaires. Implications géodynamiques. *Comptes Rendus de l'Académie des Sciences, Paris* **304**, 169–74.
- AGHZER, A. M. & ARENAS, R. 1998. Evolution métamorphique des métapelites du Massif hercynien des Rehamna (Maroc): implications tectonothermales. *Journal of African Earth Sciences* **27**, 87–106.
- AJAJI, T., WEIS, D., GIRET, A. & BOUABDELLAH, M. 1998. Coeval potassic and sodic calc-alkaline series in the postcollisional Variscan Tanncherfi intrusive complex, north-eastern Morocco: Geochemical, isotopic and geochronological evidence. *Lithos* **45**, 371–93.
- AYERS, J. 1998. Trace element modelling of aqueous fluid–peridotite interaction in the mantle wedge of subduction zones. *Contributions to Mineralogy and Petrology* **132**, 390–404.
- BARBARIN, B. 1996. Genesis of the two main types of peraluminous granitoids. *Geology* **24**, 295–98.
- BARKER, F., WONES, D. R., SHARP, W. N. & DESBOROUGH, G. A. 1975. The Pikes Peak Batholith, Colorado Front Range, and a model for the origin of the gabbro-anorthosite-syenite potassic granite suite. *Precambrian Research* **2**, 97–160.
- BARRAT, J. A., KELLER, F., AMOSSÉ, J., TAYLOR, R. N., NESBITT, R. W. & HIRATA, T. 1996. Determination of rare earth elements in sixteen silicate reference samples by ICP-MS after Tm addition and ion exchange separation. *Geostandards Newsletter* **20**, 133–40.
- BAUDIN, T., CHEVREMONT, P., RAZIN, P., THIEBLEMONT, D., RACHDI, H., ROGER, J., BENHAOURCH, R. & WINCKEL, A. 2001. Carte Géologique du Maroc au 1/50 000. Feuille d'Oulmès. *Notes et Mémoires Service Géologique Maroc* **410 bis**, 1–77.
- BAUDIN, T., CHEVREMONT, P., RAZIN, P., YUBI, N., ANDRIES, D., HOEPFFNER, C., THIEBLEMONT, D., CHIHANI, E. M. & TEGYEY, M. 2002. Carte géologique du Maroc au 1/50 000, feuille de Skhour des Rehamna, Mémoire explicatif. *Notes et Mémoires Service Géologique Maroc* **435**, 1–114.
- BEARD, J. S. & LOFGREN, G. E. 1991. Dehydration melting and water-saturated melting of basaltic and andesitic greenstones and amphibolites at 1, 3, and 6.9 kb. *Journal of Petrology* **32**, 365–401.
- BEAUCHAMP, J. 1984. Le carbonifère inférieur des Jebilet et de l'Atlas de Marrakech (Maroc): migration et comblement d'un bassin marin. *Bulletin de la Société Géologique de France* **7**, 1025–32.
- BEAUCHAMP, J., IZART, A. & PIQUÉ, A. 1991. Les bassins d'avant pays de la chaîne hercynienne au Carbonifère inférieur. *Canadian Journal of Earth Sciences* **28**, 2024–41.
- BÉDARD, J. 1990. Enclaves from the A-Type Granite of the Mégantic Complex, White Mountain Magma Series: clues to Granite Magma genesis. *Journal of Geophysical Research* **95**, 17797–819.
- BELKABIR, A., MARCOUX, E., GIBSON, H., LENTZ, D. & RZIKI, S. 2008. Geology and wall rock alteration at the Hercynian Draa Sfar Zn–Pb–Cu massive sulphide deposit, Morocco. *Ore Geology Reviews* **33**, 2–306.
- BEN ABOU, M., SOULA, J. C., BRUSSET, S., RODDAZ, M., NTARMOUCHANT, A., DRIOUCH, Y., CHRISTOPHOUL, F., BOUABDELLI, M., MAJESTÉ-MENJOUAS, C., BÉZIAT, D., DEBAT, P. & DÉRAMOND, J. 2001. Contrôle tectonique de la sédimentation dans le système de bassins d'avant-pays de la Meseta marocaine. *Comptes Rendus de l'Académie des Sciences, Paris* **332**, 703–9.
- BERNARD-GRIFFITHS, J., PEUCAT, J. J., SHEPPARD, S. M. F. & VIDAL, P. 1985. Petrogenesis of Hercynian leucogranites from the southern Armorican massif: contribution of REE and isotopic Sr, Nd, Pb and O geochemical data to the study of source rock characteristics and ages. *Earth and Planetary Science Letters* **74**, 235–50.
- BERNARDIN, C., CORNÉE, J. J., CORSINI, M., MAYOL, S., MULLER, J. & TAYEBI, M. 1988. Variations d'épaisseur du Cambrien moyen en Meseta marocaine occidentale: signification géodynamique des données de surface et de subsurface. *Canadian Journal of Earth Sciences* **25**, 2104–17.
- BONIN, B. 1996. A-type granite ring complexes: mantle origin through crustal filters and the anorthosite–rapakivi magmatism connection. In *Petrology and Geochemistry of Magmatic Suites of Rocks in Continental and Oceanic Crusts. A Volume Dedicated to Professor Jean Michot* (ed D. Demaiffe), pp. 201–18. Université Libre de Bruxelles, Royal Museum for Central Africa, Tervuren.
- BORDONARO, M., GAILLET, J. L. & MICHARD, A. 1979. Le géosynclinal carbonifère sud-mésétien dans les Jebilet (Maroc): une corrélation avec la province pyriteuse du Sud de l'Espagne. *Comptes Rendus de l'Académie des Sciences, Paris* **288**, 1371–4.
- BOULOTON, J. 1992. Mise en évidence de cordiérite héritée des terrains traversés dans le pluton granitique des Oulad Ouaslam (Jebilet, Maroc). *Canadian Journal of Earth Sciences* **29**, 658–68.
- BOULOTON, J. & GASQUET, D. 1995. Melting and undercooled crystallisation of felsic xenoliths from minor intrusions (Jebilet massif, Morocco). *Lithos* **35**, 201–19.
- BOUMMANE, M. H. & OLIVIER, PH. 2007. The Oulad Ouaslam Variscan granitic pluton (Jebilet Massif, Southwestern Moroccan Meseta): a forcibly emplaced laccolithic intrusion characterized by its magnetic and magmatic fabrics. *Journal of African Earth Sciences* **47**, 49–61.
- BUSSY, F., HERNANDEZ, J. & VON RAUMER, J. 2000. Bimodal magmatism as a consequence of the post-collisional readjustment of the thickened Variscan continental lithosphere (Aiguilles Rouges - Mont Blanc Massifs, Western Alps). *Transactions of the Royal Society of Edinburgh: Earth Sciences* **91**, 221–33.
- CHALOT-PRAT, F. 1995. Genesis of rhyolitic ignimbrites and lavas from distinct sources at a deep crustal level: field, petrographic, chemical and isotopic-Sr, Nd constraints in the Tazekka volcanic complex, Eastern Morocco. *Lithos* **36**, 29–49.

- CHAPPELL, B. W. & WHITE, A. J. R. 1974. Two contrasting granite types. *Pacific Geology* **8**, 173–4.
- CLEMENS, J. D. 1986. Origin of an A-type granite: experimental constraints. *American Mineralogist* **71**, 317–24.
- COLLINS, W. J., BEAMS, S. D., WHITE, A. J. R. & CHAPPELL, B. W. 1982. Nature and origin of A-type granites with particular reference to Southern Australia. *Contributions to Mineralogy and Petrology* **80**, 189–200.
- CREASER, R. A., PRICE, R. C. & WORMALD, R. J. 1991. A-type granites revisited: assessment of a residual-source model. *Geology* **19**, 163–6.
- DAVIES, J. H. & VON BLANCKENBURG, F. 1995. Slab break-off: a model of lithosphere detachment and its test in the magmatism and deformation of collisional orogens. *Earth and Planetary Science Letters* **129**, 85–102.
- DEPAOLO, D. 1981a. Neodymium isotopes in the Colorado Front Range and crust-mantle evolution in the Proterozoic. *Nature* **291**, 193–6.
- DEPAOLO, D. J. 1981b. Trace element and isotopic effects of combined wallrock assimilation and fractional crystallization. *Earth and Planetary Science Letters* **53**, 189–202.
- DIOT, H. & BOUCHEZ, J. L. 1989. Les granitoïdes hercyniens de la haute Moulouya: leur structure primaire déduite de l'ASM. Indications sur leur mise en place. *Bulletin de la Société Géologique de France* **4**, 705–71.
- DOSTAL, J., KEPPIE, J. D., HAMILTON, M. A., AARAB, E. M., LEFORT, J. P. & MURPHY, J. B. 2005. Crustal xenoliths in Triassic lamprophyre dykes in western Morocco: tectonic implications for Rheic Ocean suture. *Geological Magazine* **142**, 159–72.
- EBY, N. G. 1992. Chemical subdivision of the A-type granitoids: petrogenetic and tectonic implications. *Geology* **20**, 641–4.
- EL AMRANI EL HASSANI, I. E. 1996. Petrogenèse des granitoïdes peralumineux des Jebilet centrales (Maroc): approche par l'étude des enclaves. *Bulletin Institut Scientifique Rabat* **20**, 1–23.
- EL HADI, H., SIMANCAS CABRERA, F., TAHIRI, A., GONZÁLEZ LODEIRO, F., AZOR PÉREZ, A. & MARTÍNEZ POYATOS, D. J. 2006. Comparative review of the Variscan granitoids of Morocco and Iberia: proposal of a broad zonation. *Geodinamica Acta* **19**, 103–16.
- ENGLAND, P. C. & THOMPSON, A. 1986. Some thermal and tectonic models for crustal melting in continental collision zones. In *Collision Tectonics* (eds M. P. Coward & A. C. Ries), pp. 83–94. Geological Society of London, Special Publication no. 19.
- ESSAIFI, A. 1995. Relations entre magmatisme-déformation et altération hydrothermale: l'exemple des Jebilet centrales (Hercynien, Maroc). *Mémoires Géosciences Rennes* **66**, 1–340.
- ESSAIFI, A., CAPDEVILA, R., FOURCADE, S., LAGARDE, J. L., BALLÈVRE, M. & MARIIGNAC, C. 2004a. Hydrothermal alteration, fluid flow and volume change in shear zones: the layered mafic-ultramafic Kettara intrusion (Jebilet massif, Variscan belt, Morocco). *Journal of Metamorphic Geology* **22**, 25–43.
- ESSAIFI, A., CAPDEVILA, R. & LAGARDE, J. L. 2004b. Metasomatic trondhjemites and tonalites: examples in central Jebilet Variscan (Morocco). *Journal of African Earth Sciences* **39**, 369–74.
- ESSAIFI, A. & HIBTI, M. 2008. The hydrothermal system of Central Jebilet (Variscan Belt, Morocco): a genetic association between bimodal plutonism and massive sulphide deposits. *Journal of African Earth Sciences* **50**, 188–203.
- ESSAIFI, A., LAGARDE, J. L. & CAPDEVILA, R. 2001. Deformation and displacement from shear zone patterns in the Variscan upper crust, Jebilet, Morocco. *Journal of African Earth Sciences* **32**, 335–50.
- ESSAIFI, A., POTREL, A., CAPDEVILA, R. & LAGARDE, J. L. 2003. U-Pb dating: emplacement age of the bimodal magmatism of central Jebilet (Variscan Belt, Morocco). Geodynamic implications. *Comptes Rendus Géoscience* **335**, 193–203.
- EVENSEN, N. M., HAMILTON, P. J. & O'NIONS, R. K. 1978. Rare-earth abundances in chondritic meteorites. *Geochimica Cosmochimica Acta* **42**, 1199–212.
- FALLOON, T. J., GREEN, D. H., HATTON, C. J. & HARRIS, K. L. 1988. Anhydrous partial melting of a fertile and depleted peridotite from 2 to 30 kb and application to basalt petrogenesis. *Journal of Petrology* **29**, 1257–82.
- FLOYD, P. A. 1991. Rhenohercynian sandstone chemistry. In *Developments in Sedimentary Provenance Studies* (eds A. C. Morton, S. P. Todd & P. D. W. Haughton), pp. 173–88. Geological Society of London, Special Publication no. 57.
- FOURCADE, S., CAPDEVILA, R., OUABADI, A. & MARTINEAU, F. 2001. The origin and geodynamic significance of the Alpine cordierite-bearing granitoids of northern Algeria. A combined petrological, mineralogical, geochemical and isotopic (O, H, Sr, Nd) study. *Lithos* **57**, 187–216.
- FROST, B. R., BARNES, C. G., COLLINS, W. J., ARCULUS, R. J., ELLIS, D. J. & FROST, C. D. 2001. A geochemical classification for granitic rocks. *Journal of Petrology* **42**, 2033–48.
- GASQUET, D., LETERRIER, J., MRINI, Z. & VIDAL, P. 1992. Petrogenesis of the Variscan Tichka Plutonic Complex, Western High Atlas, Morocco: trace element and Rb–Sr and Sm–Nd isotopic constraints. *Earth and Planetary Science Letters* **108**, 29–44.
- GASQUET, D., STUSSI, J. M. & NACHIT, H. 1996. Les granitoïdes hercyniens du Maroc dans le cadre de l'évolution géodynamique régionale. *Bulletin de la Société Géologique de France* **167**, 517–28.
- HARRIS, N. B. W., PEARCE, J. A. & TINDLE, A. G. 1986. Geochemical characterization of collision-zone magmatism. In *Collision Tectonics* (eds M. P. Coward & A. C. Ries), pp. 67–81. Geological Society of London, Special Publication no. 19.
- HELZ, R. T. 1976. Phase relations of basalts in their melting ranges at P = 5 kb. Part II. Melt compositions. *Journal of Petrology* **17**, 139–93.
- HOEPFFNER, C., SOULAIMANI, A. & PIQUÉ, A. 2005. The Moroccan hercynides. *Journal of African Earth Sciences* **43**, 144–65.
- HOLLAND, T. & BLUNDY, J. 1994. Non-ideal interactions in calcic amphiboles and their bearing on amphibole-plagioclase thermometry. *Contributions to Mineralogy and Petrology* **116**, 433–47.
- HOLLOWAY, J. R. & BURNHAM, C. W. 1972. Melting relations of basalt with equilibrium water pressure less than total pressure. *Journal of Petrology* **13**, 1–29.
- HOUSEMAN, G. A., MCKENZIE, D. P. & MOLNAR, P. 1981. Convective instability of a thickened boundary layer and its relevance for the thermal evolution of continental convergent belts. *Journal of Geophysical Research* **86**, 6115–32.
- HUANG, H. Q., LI, X. H., LI, W. X. & LI, Z. X. 2011. Formation of high $\delta^{18}\text{O}$ fayalite-bearing A-type granite by high temperature melting of granulitic metasedimentary rocks, southern China. *Geology* **39**, 903–6.

- HUVELIN, P. 1977. Etude géologique et gîtologique du massif hercynien des Jebilet (Maroc occidental). *Notes et Mémoires Service Géologique Maroc* **232 bis**, 1–307.
- JIANG, Y. H., ZHAO, P., ZHOU, Q., LIAO, S. Y. & GIN, G. D. 2009. Middle to late Jurassic felsic and mafic magmatism in southern Hunan province, southeast China. Implications for continental arc to rifting. *Lithos* **107**, 185–204.
- KEPPLER, H. 1996. Constraints from partitioning experiments on the compositions of subduction-zone fluids. *Nature* **380**, 237–40.
- KERR, A. & FRYER, B. J. 1993. Nd isotope evidence for crust-mantle interaction in the generation of A-type granitoid suites in Labrador, Canada. *Chemical Geology* **104**, 439–60.
- LAGARDE, J. L. 1989. Granites tardi carbonifères et déformation crustale: l'exemple de la meseta marocaine. *Mémoires et Documents du Centre Armoricaïn d'Etude Structurale des Socles* **26**, 1–342.
- LAGARDE, J. L., AÏT OMAR, S. & RODDAZ, B. 1990. Structural characteristics of syntectonic plutons with special reference to late carboniferous plutons from Morocco. *Journal of Structural Geology* **12**, 805–21.
- LAGARDE, J. L., CAPDEVILA, R. & FOURCADE, S. 1992. Granites et collision continentale: l'exemple des granitoïdes carbonifères dans la chaîne hercynienne ouest-européenne. *Bulletin de la Société Géologique de France* **163**, 597–610.
- LAGARDE, J. L. & CHOUKROUNE, P. 1982. Cisaillement ductile et granitoïdes syntectoniques: l'exemple du massif hercynien des Jebilet (Maroc). *Bulletin de la Société Géologique de France* **7**, 299–307.
- LAGARDE, J. L. & MICHARD, A. 1986. Stretching normal to the regional thrust displacement in a thrust-wrench shear zone, Rehamna massif, Morocco. *Journal of Structural Geology* **8**, 483–92.
- LAMB, S., HOKE, L., KENNAN, L. & DEWEY, J. 1997. Cenozoic evolution of the central Andes in Bolivia and northern Chile. In *Orogeny Through Time* (eds J. P. Burg & M. Ford), pp. 237–64. Geological Society of London, Special Publication no. 121.
- LANDENBERGER, B. & COLLINS, W. J. 1996. Derivation of A-type granites from a dehydrated charnokitic lower crust: evidence from the Chaelundi complex, Eastern Australia. *Journal of Petrology* **37**, 145–70.
- LE CORRE, C. & BOULOTON, J. 1987. Un modèle de 'structure en fleur' associant décrochement et convergence: Les Jebilet centro-occidentales (Maroc hercynien). *Comptes Rendus de l'Académie des Sciences, Paris* **13**, 751–5.
- LE CORRE, C. & SAQUAQUE, A. 1987. Comportement d'un système pluton-encaissant dans un champ de déformation régional: le granite de Bramram (Jebilet, Maroc hercynien). *Bulletin de la Société Géologique de France* **4**, 665–73.
- LEAT, P. T., JACKSON, S. E., THORPE, R. S. & STILLMAN, C. J. 1986. Geochemistry of bimodal basalt-subalkaline/peralkaline rhyolite provinces within the Southern British Caledonides. *Journal of the Geological Society of London* **143**, 259–73.
- LINDSLEY, D. H. & ANDERSEN, D. J. 1983. A two pyroxene thermometer. Proceedings of the 13th Lunar and Planetary Science Conference, Part 2. *Journal of Geophysical Research* **8**, supplement A, 887–906.
- LITVINOVSKY, B. A., JAHN, B. M., ZANVILEVICH, A. N., SAUNDERS, A., POULAIN, S., KUZMIN, D. V., REICHOW, M. K. & TITOV, A. V. 2002. Petrogenesis of syenite-granite suites from the Bryansky Complex (Transbaikalia, Russia): implications for the origin of A-type granitoid magmas. *Chemical Geology* **189**, 105–33.
- LOOSVELD, R. J. H. & ETHERIDGE, M. A. 1990. A model for low-pressure metamorphism during crustal thickening. *Journal of Metamorphic Geology* **8**, 257–67.
- MAHÉO, G., GUILLOT, J., Blichert-Toft, Y., ROLLAND, Y. & PECHER, A. 2002. A slab break-off model for the Neogene thermal evolution of South Karakorum and South Tibet. *Earth and Planetary Science Letters* **195**, 45–58.
- MAHMOOD, A. & BENNANI, A. 1984. S-type characteristics of the Hercynian granitoids of the Central Paleozoic massif, Morocco. *Geological Magazine* **121**, 301–9.
- MAYOL, S. & MULLER, J. 1985. Mise en évidence d'une unité allochtone hercynienne précoce (antéscistiveuse) dans les Jebilet occidentales (Maroc). Etude de structuration de la zone de contact. *Comptes Rendus de l'Académie des Sciences, Paris* **300**, 369–72.
- MCBIRNEY, A. 1989. The skaergaard layered series: I. structure and average compositions. *Journal of Petrology* **30**, 363–97.
- MICHARD, A. 1976. Eléments de géologie marocaine. *Notes et Mémoires Service Géologique Maroc* **252**, 1–458.
- MICHARD, A., SOULAIMANI, A., HOEPFFNER, C., OUANAÏMI, H., BAIDDER, L., RJIMATI, E. C. & SADDIQUI, O. 2010. The South-Western branch of the Variscan Belt: evidence from Morocco. *Tectonophysics* **492**, 1–24.
- MINGRAM, B., TRUMBULL, R. B., LITTMAN, S. & GERSTENBERGER, H. 2000. A petrogenetic study of anorogenic felsic magmatism in the Cretaceous Paresis ring complex, Namibia: evidence for mixing of crust and mantle-derived components. *Lithos* **54**, 1–22.
- MITJAVILA, J., MARTI, J. & SORIANO, C. 1997. Magmatic evolution and tectonic setting of the Iberian Pyrite Belt volcanism. *Journal of Petrology* **38**, 727–55.
- MIYASHIRO, A. 1974. Volcanic rock series in island arcs and active continental margins. *American Journal of Science* **274**, 321–55.
- MORENO, C., SÁEZ, R., GONZÁLEZ, F., ALMODÓVAR, G., TOSCANO, M., PLAYFORD, G., ALANSARI, A., RZIKI, S. & BAJDDI, A. 2008. Age and depositional environment of the Draa Sfar massive sulphide deposit, Morocco. *Mineralium Deposita* **43**, 891–911.
- MIRINI, Z., RAFI, A., DUTHOU, J. L. & VIDAL, P. 1992. Chronologie Rb-Sr des granitoïdes hercyniens du Maroc: conséquences. *Bulletin de la Société Géologique de France* **163**, 281–91.
- MUSHKIN, A., NAVON, O., HALICZ, L., HARTMANN, G. & STEIN, M. 2003. The petrogenesis of A-type magmas from the Amram Massif, southern Israel. *Journal of Petrology* **44**, 815–32.
- NELSON, K. D. 1992. Are crustal thickness variations in old mountain belts like the Appalachians a consequence of lithospheric delamination? *Geology* **20**, 498–502.
- PATIÑO DOUCE, A. E. 1997. Generation of metaluminous A-type granites by low-pressure melting of calc-alkaline granitoids. *Geology* **25**, 743–6.
- PEARCE, J. A. 1983. The role of sub-continental lithosphere in magma genesis at destructive plate margins. In *Continental Basalts and Mantle Xenoliths* (eds C. J. Hawkesworth & M. J. Norry), pp. 230–49. Nantwich: Shiva.
- PEARCE, J. A., HARRIS, N. B. W. & TINDLE, A. G. 1984. Trace element discrimination diagrams for the tectonic interpretation of granitic rocks. *Journal of Petrology* **25**, 923–56.
- PIQUÉ, A., BOSSIÈRE, G., BOUILLIN, J. P., CHALLOUAN, A. & HOEPFFNER, C. 1993. Southern margin of the variscan belt: the north-western Gondwana mobile zone

- (Eastern Morocco and Northern Algeria). *Geologische Rundschau* **82**, 432–9.
- PIQUÉ, A., JEANNETTE, D. & MICHARD, A. 1980. The western meseta shear zone, a major and permanent feature of the Hercynian belt in Morocco. *Journal of Structural Geology* **2**, 397–410.
- PIQUÉ, A. & MICHARD, A. 1989. Moroccan hercynides: a synopsis. The Palaeozoic sedimentary and tectonic evolution at the northern margin of west Africa. *American Journal of Science* **289**, 286–330.
- PLAYFORD, G., GONZALEZ, F., MORENO, C. & ALANSARI, A. 2008. Palynostratigraphy of the Sarhlef Series (Mississippian), Jebilet Massif, Morocco. *Micropaleontology* **54**, 89–124.
- RODDAZ, M., BRUSSET, S., SOULA, J. C., BEZIAT, D., BENABBOU, M., DEBAT, P., DRIOUCH, Y., CHRISTOPHOUL, F., NTARMOUCHANT, A. & DERAMOND, J. 2002. Foreland basin magmatism in the western Moroccan Meseta and geodynamic inferences. *Tectonics* **21**, 1043–65.
- ROLLINSON, H. 1993. *Using Geochemical Data: Evaluation, Presentation, Interpretation*. Harlow: Longman Scientific & Technical, 352 pp.
- SAMSON, S. D., HIBBARD, J. P. & WORTMAN, G. L. 1995. Nd isotopic evidence for juvenile crust in the Carolina terrane, southern Appalachians. *Contributions to Mineralogy and Petrology* **121**, 171–84.
- SEYFERTH, M. & HENK, A. 2004. Syn-convergent exhumation and lateral extrusion in continental collision zones: insights from three-dimensional numerical models. *Tectonophysics* **382**, 1–29.
- SKJERLIE, K. P. & JOHNSTON, A. D. 1993. Fluid absent melting behavior of an F-rich tonalitic gneiss at mid-crustal pressures: implications for the generation of anorogenic granites. *Journal of Petrology* **34**, 785–815.
- SPULBER, S. D. & RUTHERFORD, M. J. 1983. The origin of rhyolite and plagiogranite in oceanic crust: an experimental study. *Journal of Petrology* **24**, 1–25.
- SUN, S. & MCDONOUGH, W. F. 1989. Chemical and isotopic systematic of oceanic basalts: implications for mantle composition and processes. In *Magmatism in the Ocean Basins* (eds A. D. Saunders & M. J. Norry), pp. 313–45. Geological Society of London, Special Publication no. 42.
- TAYLOR, S. R. & MCLENNAN, S. M. 1995. The geochemical evolution of the continental crust. *Reviews of Geophysics* **33**, 241–65.
- THOMPSON, R. N., DICKIN, A. P., GIBSON, I. L. & MORRISON, M. A. 1982. Elemental fingerprints of isotopic contamination of Hebridean Palaeocene mantle-derived magmas by Archaean sial. *Contributions to Mineralogy and Petrology* **79**, 159–68.
- THORPE, R. S., LEAT, P. T., MANN, A. C., HOWELLS, M. F., REEDMAN, A. J. & CAMPBELL, D. G. 1993. Magmatic evolution of the Ordovician Snowdon volcanic centre, North Wales (UK). *Journal of Petrology* **34**, 711–4.
- TOTTEN, M. W., HANAN, M. A. & WEAVER, B. L. 2000. Beyond whole-rock geochemistry of shales: the importance of assessing mineralogic controls for revealing tectonic discriminants of multiple sediment sources for the Ouachita Mountain flysch deposits. *Geological Society of America Bulletin* **112**, 1012–22.
- TURNER, S., FODEN, J. D. & MORRISON, R. S. 1992. Derivation of some A-type magmas by fractionation of basaltic magmas: an example from the Pathdaway ridge, South Australia. *Lithos* **28**, 151–79.
- TURNER, S., PLATT, J. P., GEORGE, R. M. M., KELLY, S. P., PEARSON, D. G. & NOWELL, G. M. 1999. Magmatism associated with orogenic collapse of the Betic-Alboran Domain, SE Spain. *Journal of Petrology* **40**, 1011–36.
- VOGEL, T. A., WILLIAMS, E. R., PRESTON, J. K. & WALKER, B. M. 1976. Origin of the late Palaeozoic plutonic massifs in Morocco. *Geological Society of America Bulletin* **87**, 1753–62.
- VON RAUMER, J. F., BUSSY, F. & STAMPFLI, G. M. 2009. The Variscan evolution in the External Massifs of the Alps and place in their Variscan framework. *Comptes Rendus Geosciences* **341**, 239–52.
- VON RAUMER, J. F. & STAMPFLI, G. M. 2008. The birth of the Rheic Ocean: early Palaeozoic subsidence patterns and subsequent tectonic plate scenarios. *Tectonophysics* **46**, 9–20.
- WANG, K. L., CHUNG, S. L., O'REILLY, S. Y., SUN, S. S., SHINJO, R. & CHEN, C. H. 2004. Geochemical constraints for the genesis of postcollisional magmatism and the geodynamic evolution of the northern Taiwan region. *Journal of Petrology* **45**, 975–1011.
- WATSON, E. B. & HARRISON, T. M. 1983. Zircon saturation revisited: temperature and composition effects in a variety of crustal magma types. *Earth and Planetary Science Letters* **64**, 295–304.
- WHALEN, J. B., CURRIE, K. L. & CHAPPELL, B. W. 1987. A-type granites: geochemical characteristics, discrimination and petrogenesis. *Contributions to Mineralogy and Petrology* **95**, 407–19.
- WHALEN, J. B., MCNICOLL, V. J., VAN STAAL, C. R., LISSEBERG, C. J., LONGSTAFFE, F. J., GENNER, G. A. & VAN BREEMAN, O. 2006. Spatial, temporal and geochemical characteristics of Silurian collision-zone magmatism, Newfoundland Appalachians: an example of a rapidly evolving magmatic system related to slab break-off. *Lithos* **89**, 377–404.
- WICKHAM, S. M., ALBERTS, A. D., ZANVILEVICH, A. N., LITVINOVSKY, B. A., BINDEMAN, I. N. & SCHAUBLE, E. A. 1996. A stable isotope study of anorogenic magmatism in East Central Asia. *Journal of Petrology* **37**, 1063–95.
- WILSON, M. 1989. *Igneous Petrogenesis*. London: Unwin Hyman, 456 pp.
- WINCHESTER, J. A. & FLOYD, P. A. 1976. Geochemical magma type discrimination: application to altered and metamorphosed basic igneous rocks. *Earth and Planetary Science Letters* **28**, 459–69.
- WOOD, D. A. 1980. The application of a Th–Hf–Ta diagram to problems of tectonomagmatic classification and to establishing the nature of crustal contamination of basaltic lavas of the British Tertiary volcanic province. *Earth and Planetary Science Letters* **50**, 11–30.
- YANG, J. H., WU, F. Y., CHUNG, S. L., WILDE, S. A. & CHU, M. F. 2006. A hybrid origin for the Qianshan A-type granite, Northeast China: geochemical and Sr–Nd–Hf isotopic evidence. *Lithos* **89**, 89–106.